AD-A126 098 SOLID-STATE LASERS FOR BATHYMETRY AND COMMUNICATIONS STUDIES OF FOUR RARE..(U) NAVAL AIR DEVELOPMENT CENTER WARMINSTER PA SENSORS AND AVIONI.. M B RANKIN ET AL. 1/1

UNCLASSIFIED 03 JAN 83 NADC-83009-30 F/G 20/5 NL

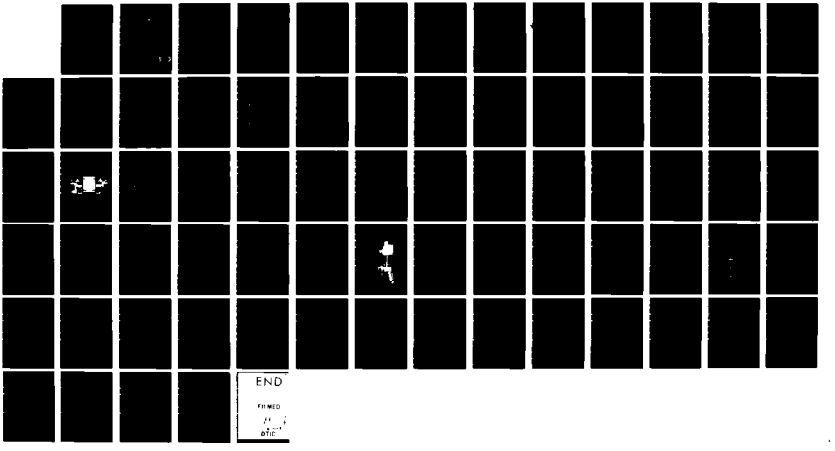

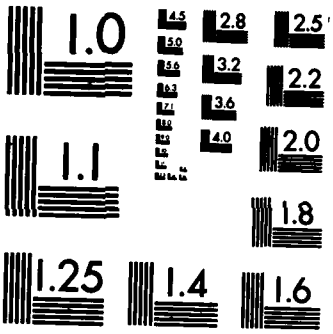

(12)

REPORT NO. NADC-83009-30

AD A126098

SOLID-STATE LASERS FOR BATHYMETRY AND COMMUNICATIONS

STUDIES OF FOUR RARE-EARTH MATERIALS

Michael B. Rankin
Gerald D. Ferguson
Stephen R. Bazow
Sensors and Avionics Technology Directorate
NAVAL AIR DEVELOPMENT CENTER
Warminster, PA 18974

3 JANUARY 1983

FINAL REPORT
Program Element 61152N
Task Area RO1107
Work Unit GC102

Approved For Public Release; Distribution Unlimited

Prepared For
Chief of Naval Material (MAT-052)
Department of the Navy
Washington, DC 20360

NOTICES

REPORT NUMBERING SYSTEM – The numbering of technical project reports issued by the Naval Air Development Center is arranged for specific identification purposes. Each number consists of the Center acronym, the calendar year in which the number was assigned, the sequence number of the report within the specific calendar year, and the official 2-digit correspondence code of the Command Office or the Functional Directorate responsible for the report. For example: Report No. NADC-78015-20 indicates the fifteenth Center report for the year 1978, and prepared by the Systems Directorate. The numerical codes are as follows:

CODE	OFFICE OR DIRECTORATE
00	Commander, Naval Air Development Center
01	Technical Director, Naval Air Development Center
02	Comptroller
10	Directorate Command Projects
20	Systems Directorate
30	Sensors & Avionics Technology Directorate
40	Communication & Navigation Technology Directorate
50	Software Computer Directorate
60	Aircraft & Crew Systems Technology Directorate
70	Planning Assessment Resources
80	Engineering Support Group

PRODUCT ENDORSEMENT – The discussion or instructions concerning commercial products herein do not constitute an endorsement by the Government nor do they convey or imply the license or right to use such products.

APPROVED BY: Gino K Wilt DATE: 3/2/83

UNCLASSIFIED

SECURITY CLASSIFICATION OF THIS PAGE (When Data Entered)

REPORT DOCUMENTATION PAGE		READ INSTRUCTIONS BEFORE COMPLETING FORM
1. REPORT NUMBER NADC-83009-30	2. GOVT ACCESSION NO. AD-A126	3. RECIPIENT'S CATALOG NUMBER 098
4. TITLE (and Subtitle) Solid-State Lasers For Bathymetry And Communications, Studies Of Four Rare-Earth Materials		5. TYPE OF REPORT & PERIOD COVERED FINAL REPORT Oct 1979-Sep 1981
		6. PERFORMING ORG. REPORT NUMBER
7. AUTHOR(s) Michael B. Rankin, Gerald D. Ferguson, and Stephen R. Bazow		8. CONTRACT OR GRANT NUMBER(s) N/A
9. PERFORMING ORGANIZATION NAME AND ADDRESS Sensors and Avionics Technology Directorate Code 3011 Naval Air Development Center Warminster, PA 18974		10. PROGRAM ELEMENT, PROJECT, TASK AREA & WORK UNIT NUMBERS P.E.: 61152N Project No. ZR00001 T.A. No. ZR01107. W.U. No. GC-102
11. CONTROLLING OFFICE NAME AND ADDRESS CHIEF OF NAVAL MATERIAL Department of the Navy (CODE MAT-052) Washington, DC 20360		12. REPORT DATE 3 Jan 1983 13. NUMBER OF PAGES 68
14. MONITORING AGENCY NAME & ADDRESS(if different from Controlling Office)		15. SECURITY CLASS. (of this report) UNCLASSIFIED 15a. DECLASSIFICATION/DOWNGRADING SCHEDULE N/A

16. DISTRIBUTION STATEMENT (of this Report)

Approved For Public Release; Distribution Unlimited

17. DISTRIBUTION STATEMENT (of the abstract entered in Block 20, if different from Report)

18. SUPPLEMENTARY NOTES

19. KEY WORDS (Continue on reverse side if necessary and identify by block number)

Blue-Green Lasers	Nd:YAG
Solid-State Lasers	Li Ho F_4
Rare-Earth Laser Materials	Li Tb F_4
Near-IR Lasing Transitions	Er:Li YF_4
Refrigerated Laser Materials	Bathymetry Lasers

20. ABSTRACT (Continue on reverse side if necessary and identify by block number)

Lasing transitions of four rare-earth ions in crystalline hosts were investigated for use in laser bathymetry and strategic communications systems. Transitions in Nd:YAG ($^4F_{3/2} \rightarrow {}^4I_{9/2}$ at 946 nm) and Li Ho F_4 ($^5F_5 \rightarrow {}^5I_7$ at 979 nm) were studied theoretically and experimentally from 210K to 273K. At 210K the Nd transition produced 42 mj of energy when pumped by a krypton lamp with 32 joules of energy. The stimulated emission cross-section of the transition in Li Ho F_4 was found to be 4×10^{-20} cm^2. The lasing threshold of a 5 mm x 75 mm Hi Ho F_4 rod exceeded 50 joules at 210K. Lasing was not observed in this material. The cross-section of the $^5D_4 \rightarrow {}^7F_5$

DD FORM 1 JAN 73 1473 EDITION OF 1 NOV 65 IS OBSOLETE
S/N 0102-LF-014-6601

UNCLASSIFIED

SECURITY CLASSIFICATION OF THIS PAGE (When Data Entered)

.16 x 10 to the -20th power sq. cm.

UNCLASSIFIED

SECURITY CLASSIFICATION OF THIS PAGE (When Data Entered)

Block 20. (continued)

transition (545 nm) in Li Tb F_4 was measured as 1.6×10^{-21} cm^2 at 77K. The cross-section of the $^4S_{3/2} \rightarrow {}^4I_{15/2}$ transition (550 nm) in Er: Li YF_4 was measured as 5×10^{-20} cm^2 at 77K. A first-order analysis of the efficiency of refrigerated solid-state lasers is presented. The frequency-doubled Nd:YAG laser at 532 nm appears more efficient than any of the transitions studied in this work.

5 x 10 to the -20th power sq cm

TABLE OF CONTENTS

LIST OF FIGURES

LIST OF TABLES

This Page Intentionally Left Blank

EXECUTIVE SUMMARY

Introduction

Low-temperature lasing transitions in the solid-state materials Nd:YAG (946 nm), $LiHoF_4$ (979 nm), $LiTbF_4$ (545 nm) and Er:$LiYF_4$ (550 nm) were evaluated for use in two naval system applications: shallow-water laser bathymetry (depth measurement) and satellite-to-submarine optical communications. The objective was to identify a lasing transition capable of performance superior to frequency-doubled Nd:YAG at 532 nm for each application.

Background

Shallow-water bathymetry systems presently in development will require high repetition rate, low pulse energy transmitters emitting in the 510-550 nm spectral range. Satellite-to-submarine communications systems will require much larger pulse energies at lower repetition rates in the 470-490 nm range. Presently, the frequency-doubled Nd:YAG laser at 532 nm represents the best solid-state laser for either application. The two near-IR transitions, 946 nm and 979 nm, when frequency-doubled, produce wavelengths quite close to the optimum for communications systems. The two visible transitions, 545 nm and 550 nm, are useful for bathymetry, and eliminate the efficiency reduction and reliability problems associated with frequency doubling. Low-temperature operation was employed as a technique to improve the efficiencies of all the materials studied.

Conclusions

1. None of the transitions studied show clear superiority over the 532-nm frequency-doubled Nd:YAG laser for either bathymetry or communications systems. Low eficiency is a major limitation for all four transitions.

2. Useful amounts of energy can be obtained at 946 nm with Nd:YAG, but at efficiencies of 0.13%, too small for the application envisioned. The reasons for this low efficiency are not entirely clear.

3. The lasing threshold of the 979-nm transition in $LiHoF_4$ exceeds 50 J at 210 K. The threshold should be lower at 77 K, but not low enough for efficient operation.

4. $LiTbF_4$ is extremely difficult to grow in the size and optical quality required for laser use. In addition, its cross section appears to be too small for efficient operation.

5. A competing process, possibly excited state absorption, interferes with the 550-nm transition in $Er:LiYF_4$. Even optimistic estimates of its performance at 77 K do not predict efficient operation.

6. An analysis of the power consumption in a refrigerated solid-state laser indicates that a lasing efficiency of at least 1% at 77 K is necessary to match the efficiency of doubled Nd:YAG because of the additional power consumed by the refrigeration apparatus.

7. Refrigeration technology is a critical area for efficient low-temperature operation. The overall efficiency of a refrigerated solid-state material depends strongly on the efficiency of the refrigeration system.

Recommendations

1. Serious consideration of low-temperature solid-state materials should be limited to candidates with the following characteristics:

   a. High efficiency: at least 1% overall for operation at 77 K.
   b. Low waste heat evolution in the lasing material.

2. A thorough study of refrigeration techniques and efficiencies for the temperature range of interest should accompany further efforts to develop low-temperature materials for field use.

3. Efficient alternatives to flashlamp pumping should be explored for low-temperature materials. The use of laser diodes to pump Nd:YAG is one such technique.

4. Further exploration of the 946-nm transition in Nd:YAG should include the dynamics of competition between the 946-nm and 1064-nm lasing transitions.

5. Oscillator-amplifier configurations should be analyzed for possible application to the 946-nm Nd:YAG transition. It may prove possible to extract more of the inversion energy at 946 nm from an amplifier than from an oscillator.

This Page Intentionally Left Blank

SECTION 1

INTRODUCTION

Four low-temperature solid-state lasing transitions were evaluated under the NAVAIRDEVCEN Independent Research Program during FY80 and FY81. The investigators studied the utility of these materials for use in two naval air-to-underwater systems. The 946-nm transition in Nd:YAG and the 979-nm transition in $LiHoF_4$ were evualated for use in optical satellite-to-submarine communications systems. The 545-nm transition in $LiTbF_4$ and the 550-nm transition in $Er:LiYF_4$ were considered for application to coastal bathymetry (depth measurement) systems employing airborne optical radar. The objective was to identify a solid-state material capable of performance superior to that of frequency-doubled Nd:YAG (wavelength: 532 nm) for each application.

The state of development of each of these materials is different, and the methods of investigation varied accordingly. The 946-nm transition in Nd:YAG and the 979-nm transition in $LiHoF_4$ were studied theoretically and experimentally at NAVAIRDEVCEN, in the temperature range 210 K - 273 K. Spectroscopic evaluation of $LiHoF_4$ was done at the Crystal Physics and Optical Electronics Laboratory (CPOEL) of the Massachusetts Institute of Technology (MIT). The study of $LiHoF_4$ and $Er:LiYF_4$ was more theoretical, and drew heavily on concurrent studies in growth and spectroscopy of these materials at the CPOEL. Since temperatures as low as 77 K were anticipated for efficient operation of some of these materials, some consequences of low-temperature, high average power operation were considered.

The laser transmitter requirements for satellite communications and coastal airborne bathymetry are summarized in table 1.1.[1] For satellite communications, large pulse energies (1 J) at moderate repetition rates (100 Hz) are required. Coastal hydrography systems require pulse engeries of millijoules at repetition rates from about 400 Hz to several thousand hertz. The spectral transmission of the water type for each system dominates the propagation losses. The spectral characteristics for coastal and offshore

TABLE 1.1

BLUE-GREEN LASER REQUIREMENTS

Laser Parameter	Satellite Communication	Airborne Hydrography	ASW Surveillance	Reason for Parameter Value
Wavelength (nm)	410 - 510	510 - 560	410 - 510	Underwater Transmission Window
Pulse Energy (mJ)	1,000	2 - 5	100	Penetration depth in water
Pulse Width (ns)	1,000	3 - 5	10 - 20	Depth Resolution
Pulse Repetition Frequency (Hz)	100	$\geq$ 400	400 - 3,000	Area Coverage or Data Rate
Average Power Output (W)	100	$\geq$ 1	$\geq$ 40	
Efficiency (%)	1	> 0.1	$\geq$ 0.5	Power, Size, and Weight Available
Mission Length	5 yr	7 hr	10 hr	Operational Requirements

waters, shown in figure 1.1, determine the optimum operating wavelength for each system. The near-IR transitions 946 nm (Nd:YAG) and 979 nm ($LiHoF_4$) were studied for satellite communications applications because their second harmonics, 473 nm and 489 nm, fall close to the optimum wavelength for communications in deep oceanic waters. This wavelength match provides a range increase over 532 nm frequency-doubled Nd:YAG for identical pulse energy. The 545-nm transition in $LiTbF_4$ and the 550 nm transition in Er:$LiYF_4$ match the optical transmission of the coastal waters in which bathymetry systems operate. These transitions present the possibility of eliminating the frequency doubling necessary in 532 nm Nd:YAG systems. Frequency doubling crystals, due to their susceptibility to optical damage, have been weak links in many YAG systems used in airborne tests in the past. The limited conversion efficiency of the crystals also reduces the efficiency attainable with YAG technology below that of the laser itself.

A practical solid-state laser material for airborne system applications must satisfy many requirements, beginning with wavelength, facility of crystal growth, and crystal mechanical and optical characteristics. The general features of the active ion energy level structure most conducive to efficient operation are shown in figure 1.2. A large pumping rate is necessary to populate the upper laser level efficiently. A long lifetime for this level allows energy storage for Q-switched operation. A large stimulated emission cross section for the lasing transition is desirable. If the lower laser level is unpopulated, more of the energy stored in the inversion can be extracted in lasing. These characteristics are present for the 1.06 μm transition in Nd:YAG, and account for its high efficiency of 1% to 2%.

The transitions described in this report do not have all these desirable characteristics at room temperatures. Cooling the material can reduce the equilibrium population of a lower level which is thermally populated at room temperature. This is the case for the 946-nm transition in Nd:YAG and the 550-nm transition in Er:$LiYF_4$. Lower temperatures can also increase the effective stimulated emission coefficient of a transition by narrowing the line shape, as in $LiTbF_4$. An objective of the project was to establish whether any of the four transitions could operate efficiently enough at reduced temperatures to compete with doubled Nd:YAG.

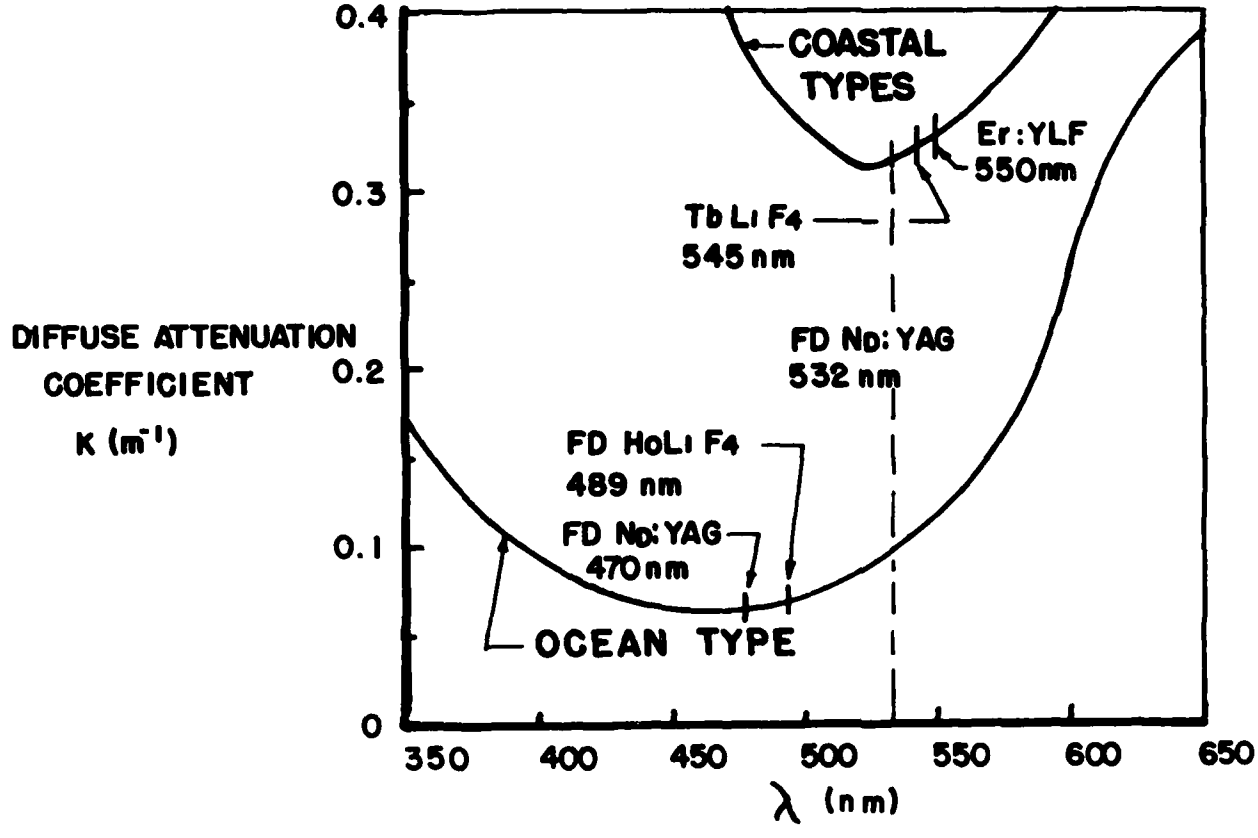

Figure 1.1. Wavelengths For Communications And Hydrography

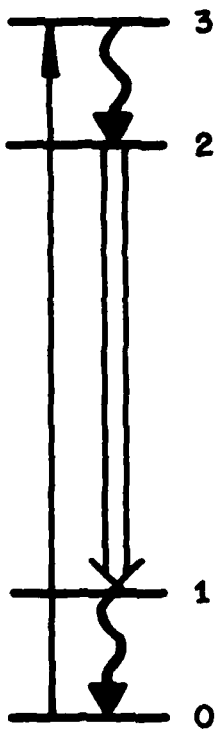

I HIGH PUMPING RATE
- AVAILABLE PUMP BANDS AND SOURCES
- RAPID TRANSFER TO UPPER LASER LEVEL

II LOWER LASER LEVEL UNPOPULATED
- THERMALLY UNPOPULATED ($E_1 \gg kT$)
- RAPID DECAY OF LOWER LASER LEVEL

III UPPER LASER LEVEL METASTABLE
- SLOWER DECAY THAN THE ABOVE
- RADIATIVE DECAY DOMINATES

Figure 1.2. Factors Leading To A Large Population Inversion

The following sections of the report detail the studies of each lasing transition. Section 2 presents theoretical modelling of the threshold behavior and above-threshold operation of the 946-nm transition $^4F_{3/2} \rightarrow {}^4I_{9/2}$ in Nd:YAG. Experimental studies of the temperature dependence of lasing threshold in the 210 K - 273 K range are described. At 210 K, pulses containing 43 mJ of energy at 946 nm were produced with an input of 32.9 J. The same rod under the same pumping conditions produced 270 mJ of energy when operated at 1.06 μm with 34.2 J input. The relative intensities and decay time constants of spontaneous emission at 1.06 μm and 946 nm in the pumped rod were measured at 210 K. The results suggest that amplified spontaneous emission at 1.06 μm and possibly excited state absorption may limit the energy available at 946 nm.

Section 3 describes the 979-nm transition in $LiHoF_4$. Initial Russian reports are summarized together with spectroscopic results obtained at the MIT CPOEL. The experimental tests of $LiHoF_4$ at NAVAIRDEVCEN, which did not produce lasing at pumping energies up to 50 J, are described.

The green-emitting transitions in $LiTbF_4$ and Er:$LiYF_4$ are covered in section 4. This section also presents a first-order analysis of the energy consumption of a refrigerated solid-state laser. A comparison of $LiTbF_4$, Er:$LiYF_4$, and frequency-doubled Nd:YAG for a hypothetical bathymetry application concludes this section.

Section 5 reviews in detail the conclusions for each material.

SECTION 2

THE 946 nm TRANSITION IN Nd:YAG

The 946-nm transition in neodymium-doped yttrium aluminum garnet (Nd:YAG) was considered initially in this project because of the close coincidence between its second harmonic, 473 nm, and the optimum wavelength for the down link of a strategic communications system. A useful transition in Nd:YAG is automatically of interest since the material lases efficiently at 1.06 μm, has good physical, thermal, and optical properties, and is readily available for experimental work. Much effort has been devoted to growth of the crystal for laser application, and its spectroscopic properties have been studied extensively. The material is mature and well-developed compared to other solid-state materials. Our investigation began with theoretical performance estimates based on known spectroscopic properties, and was completed with experimental lasing tests and fluorescence measurements.

Figure 2.1 shows the portion of the energy level structure of the Nd^{+3} ion relevant to near-IR laser operation.[2] The $^4F_{3/2}$ manifold serves as the upper laser level for some 20 lasing transitions,[3] of which the strongest is the well-known 1.06 μm transition, $^4F_{3/2} \rightarrow {}^4I_{11/2}$. The $^4F_{3/2} \rightarrow {}^4I_{9/2}$ transition at 946 nm is the strongest transition with a wavelength shorter than 1 μm. The $^4F_{3/2}$ manifold is readily excited or pumped optically with krypton or xenon-filled flashlamps. Drawing on earlier work by Wallace and Harris,[4] we identified three characteristics of the transition which are important for efficient 946 nm lasing:

1. Lasing at 1.06 μm must be suppressed, since both transitions originate from the same upper level manifold and compete for inversion energy.

2. The terminal level of the 946-nm transition has an appreciable thermal population (∿ 1%) at room temperature. Reducing this population lowers the lasing threshold.

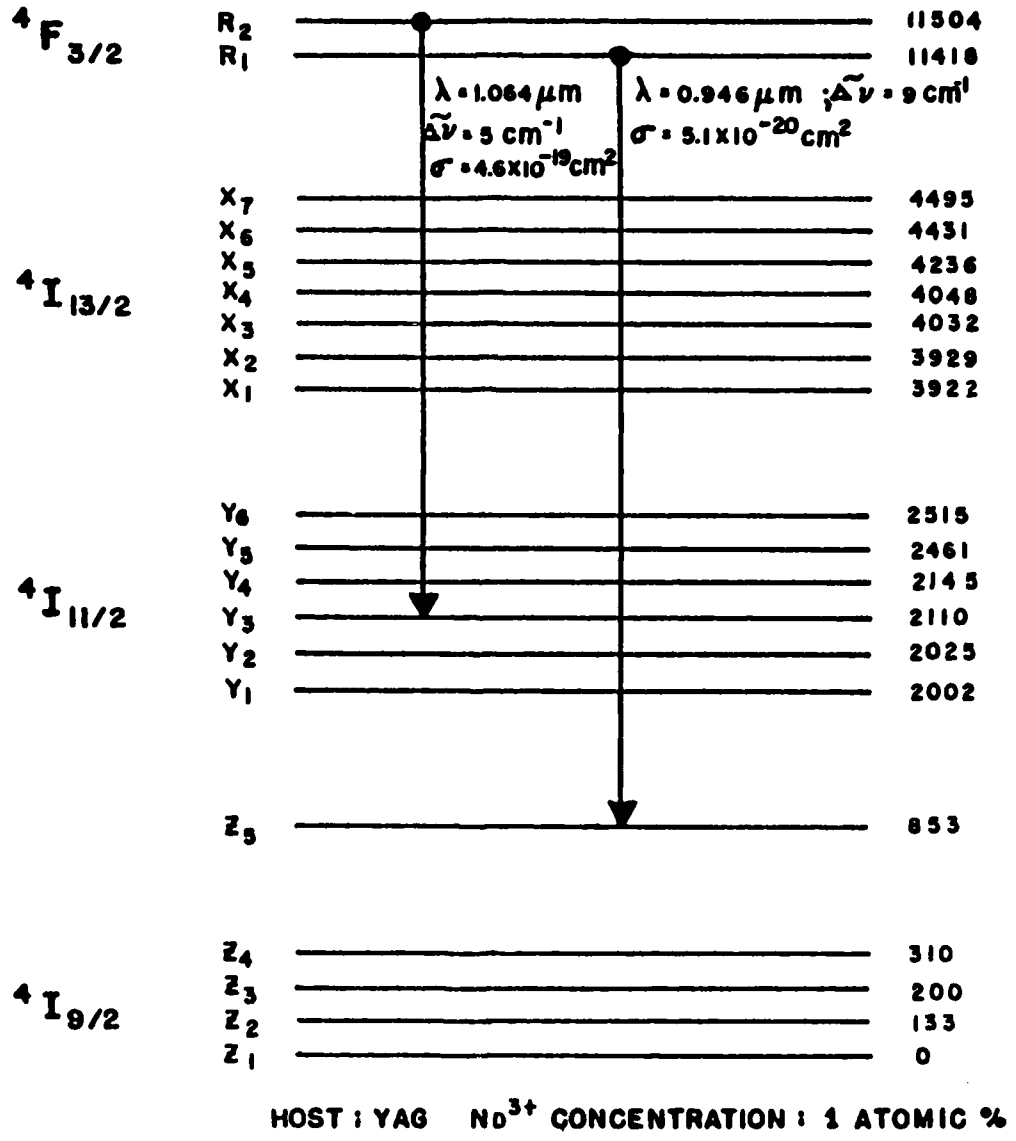

Figure 2.1. Nd: YAG Ion Energy Levels

3. The stimulated emission cross-section for the 946-nm transition is a factor of 10 smaller than the 1.06-μm cross-section.[2] In Q-switched operation, efficient extraction of inversion energy in short pulses becomes more difficult for smaller stimulated emission cross-sections.

Our approach to the design of a 946 nm laser took these characteristics of Nd:YAG into account. Suppression of 1.06-μm lasing was provided in the resonator design. The laser rod was cooled to reduce the thermal population of the terminal laser level. The technique of pulse transmission mode (PTM) Q-switching[5] was selected to extract the energy in a short pulse. Initial theoretical estimates of performance indicated that lasing thresholds of 15 J should be possible at 70°C and that as much as 200 to 300 mJ could be stored in the inversion at that temperature.

Theoretical Modelling

The ingredients of our model of the 946-nm laser are the rate of excitation (pumping) into the upper laser level, R_1 of $^4F_{3/2}$ in figure 2.1, the stimulated emission cross-sections at 946 nm and 1.06 μm, and the loss factor of the resonator at each wavelength. We assume that the relaxation time between the Stark components of an energy level is short enough to treat their populations as being in thermal equilibrium. The pumping process is assumed to be linearly related to the energy stored in the flashlamp capacitor:

$$N_U = KE \tag{2.1}$$

where

N_U = population density of upper laser level (ions/cm^3)

E = electrical energy discharged into flashlamp (joules)

K = pumping constant (ions/cm^3-joule)

The constant K includes efficiency factors for all the electrical and optical energy transfers involved in pumping the laser rod. K is a characteristic of the flashlamp network and pump cavity, and is measured experimentally. Our

method of evaluating K for the 946-nm transition is described in appendix I.A. In our experiments, K was on the order of 10^{16} ions/cm^3-joule.

The basic equation of our model predicts the threshold energy of the 946 nm transition:

$$E_t = \frac{1}{K} (N_U + N_L) \tag{2.2}$$

in which

E_t = flashlamp discharge capacitor energy required to reach threshold (joules)
K = pumping constant (ions/cm^3-joules)
N_U = upper laser level population density required for 4-level threshold (ions/cm^3)
N_L = thermal population of lower laser level (ions/cm^3)

N_U is calculated from a standard threshold equation for a 4-level laser:[6]

$$(\Delta n)_t = N_U = - \frac{1}{2\sigma\ell} (\ell n\ RT_E^2) + \frac{\alpha}{\sigma} \tag{2.3}$$

in which

$(\Delta n)_t$ = Population inversion density at threshold (ions/cm^3)
N_U = Upper laser level population density (ions/cm^3)
σ = Stimulated emission cross-section (cm^2)
ℓ = Length of active medium (cm)
R = Product of mirror reflectances
T_E = Product of single-pass transmission factors for resonator elements
α = Passive loss coefficient for laser rod (cm^{-1})

The first equality holds when the lower level of the transition is unpopulated. N_L in equation (2.2) accounts for the thermal population of the Z_5 level, and is given by:

$$N_L = \frac{N_o \exp\ (-853\ cm^{-1}/kT)}{Z(T)} \tag{2.4}$$

with

N_o = Nd^{+3} ion density in Nd:YAG, 1.38×10^{20} ions/cm^3

k = Boltmann's constant, 0.694 cm^{-1} K^{-1}

T = Temperature (K)

Z(T) = partition function for $^4I_{9/2}$ manifold

The primary temperature dependence of 946-nm threshold comes from the Z_5 population dependence in equation (2.4). The pumping constant K may have a weak temperature dependence. The temperature dependence of σ for the 946-nm transition is negligible in the temperature range considered, 0 C to -70 C.

Figure 2.2 shows threshold energies calculated from equations (2.1) through (2.4) using the numerical values of table 2.1, plotted against the temperature of the laser rod.

Output energy for operation above threshold was estimated by calculating the stored energy in excess of threshold inversion, using:

$$E_S = K(E-E_t)\ V\varepsilon \qquad (2.5)$$

with

E_S = Stored energy (joules)

E = Capacitor energy (joules)

K = Pumping constant (ions/cm^3-joule)

E_t = Threshold capacitor energy (joules)

V = Volume of laser rod (cm^3)

ε = Energy of a 946 nm photon, 2.1×10^{-19} joules

The stored energy in equation (2.5) has the temperature dependence of E_t. Figure 2.3 shows calculations of stored energy versus flashlamp input energy for temperatures of 0°C and -70°C. The parameters of table 2.1 are used in this calculation. Active volume is 6.35 cm long by 0.5 cm in diameter, or 1.25 cm^3.

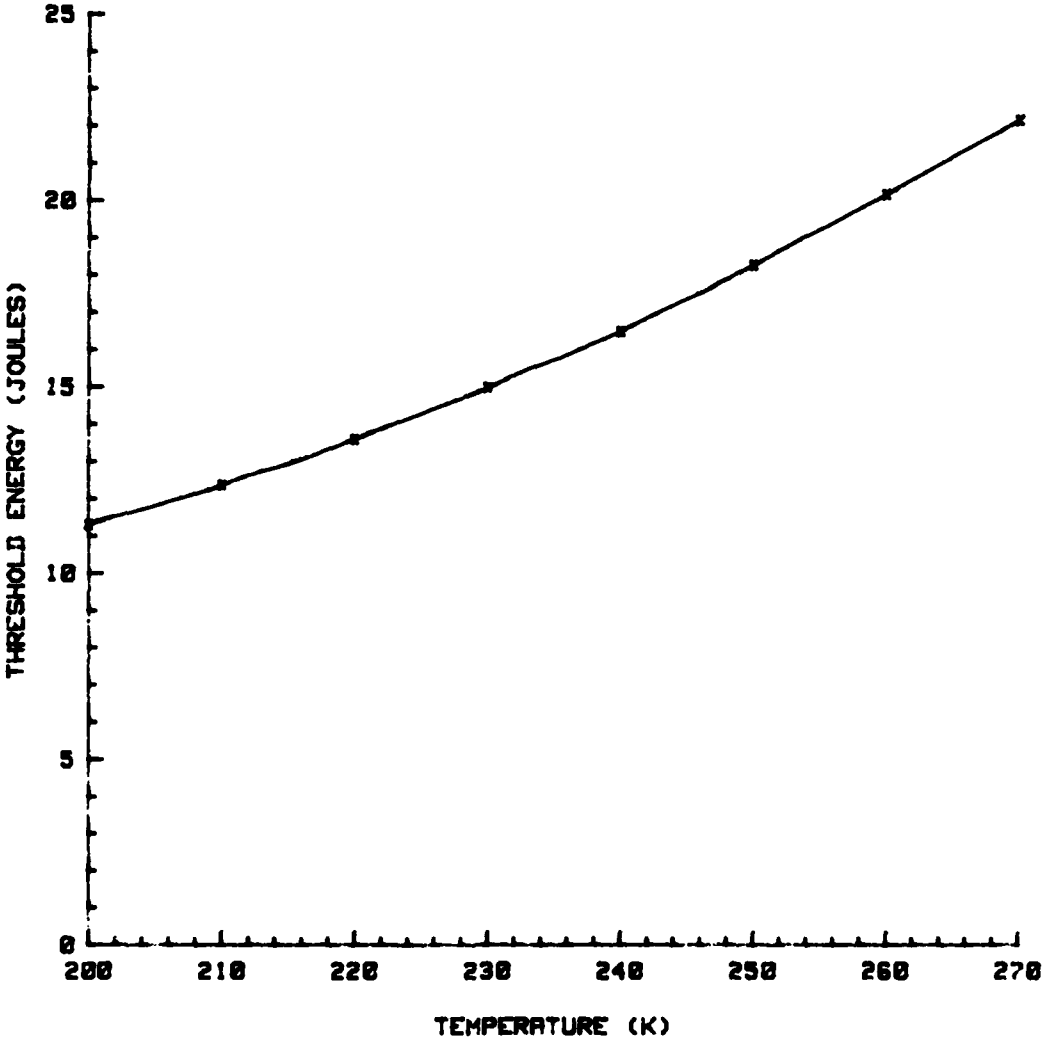

Figure 2.2. Theoretical Thresholds For 946 nm Laser With Parameters Of Table 2.1

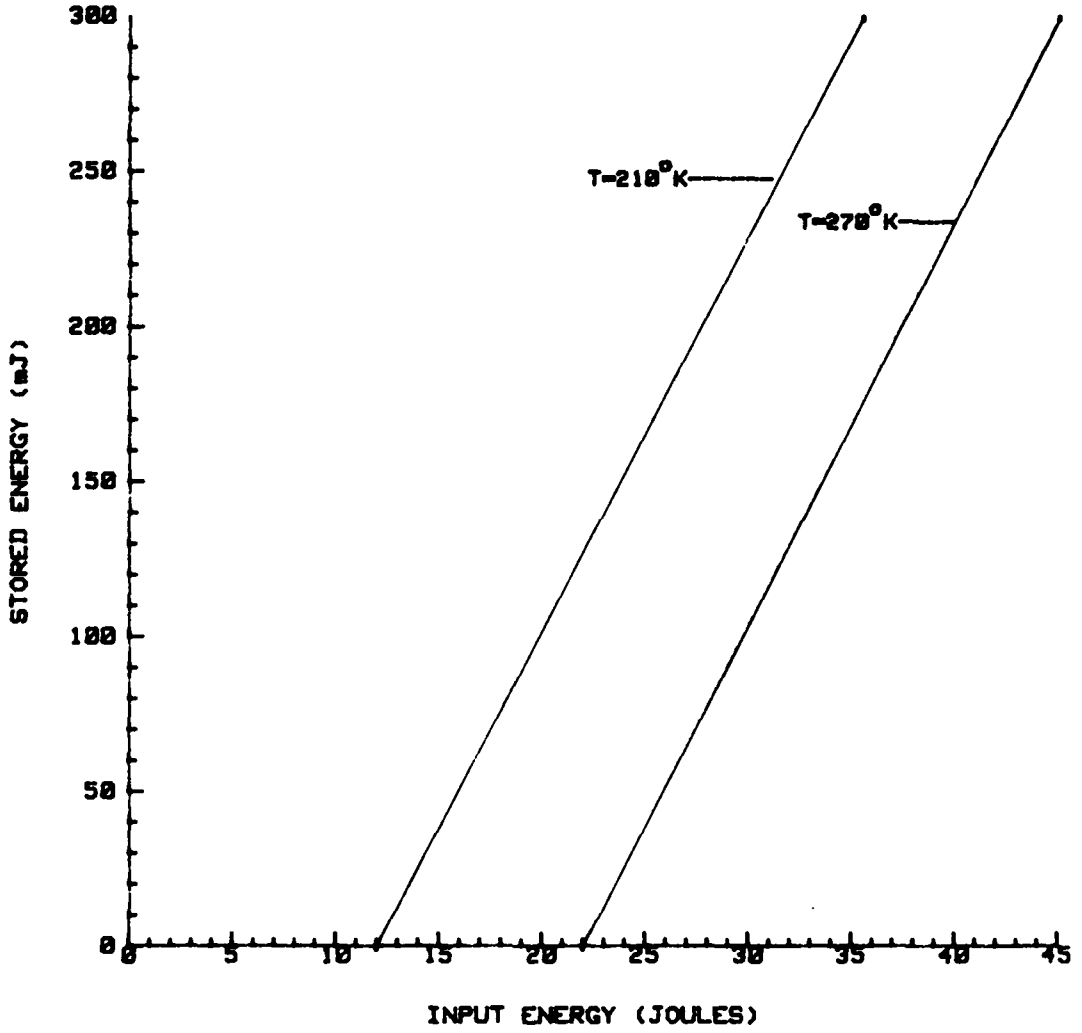

Figure 2.3. Stored Energy Versus Flashlamp Energy For 946 nm Transition

TABLE 2.1

NUMERICAL VALUES FOR 946 nm MODELLING CALCULATIONS

Parameter	Symbol, [Units]	Value
Pumping Constant	K, [ions/cm^3 - jale]	5×10^{16}
Stimulated Emission Cross-Section	σ, [cm^2]	5.1×10^{-20} (946 nm) 4.6×10^{-19} (1.06 μm)
Active Length	ℓ, [cm]	6.35
Active Volume	V, [cm^3]	1.24
Mirror Reflectance Product	R	0.98 (946 nm) 2.5×10^{-3} (1.06 μm)
Resonator Efficiency	T_E	0.9 (946 nm)
Passive Rod Loss Coefficient	α, [cm^{-1}]	2×10^{-3}

An upper limit on E is imposed by the onset of lasing at 1.06 μm, which occurs when the 1.06 μm gain equals the resonator losses. Equations (2.1) and (2.3) can be applied to the 1.06 μm transition to calculate the amount of suppression (represented by the value of RT_E^2) required to raise the threshold to a prescribed value. Results using values from table 2.1 are given in table 2.2.

TABLE 2.2

ESTIMATED 1.06 μm SUPPRESSION REQUIREMENTS

Threshold Energy (1.06 μm) [J]	Required Value of RT_E^2
30	1.52×10^{-4}
35	3.54×10^{-5}
40	8.2×10^{-6}

A 1.06-μm threshold of 30 J would allow approximately 250 mJ of energy storage in a 6.35 cm 0.5 cm laser rod. This indicates that a wavelength selectivity of at least 10^4 favoring 946 nm is necessary.

Experimental Apparatus

The pump cavity used in the experimental studies was designed to maintain a 5 mm diameter by 7.62 cm long laser rod at -70 C while being pumped by a water-cooled flashlamp with an arc length of 6.35 cm. The assembled pump cavity is shown in figure 2.4, and internal details of the cavity are shown in figure 2.5. The laser rod was enclosed by a 9 mm ID x 11 mm OD flow tube through which refrigerated alcohol circulated as coolant. A similiar flow tube conducted the flashlamp's water coolant. The interior of the pump cavity was dry. The pump cavity's reflector was a quartz elliptical cylinder with a major diameter of 3.9 cm, a minor diameter of 3.34 cm, and an eccentricity of 0.516. The outer surface was coated with evaporated silver and overcoated with chromium to prevent tarnishing. The laser rod and flashlamp were located at the foci of the ellipse, separated by 2 cm (center to center). The flow tubes in the pump cavity also served to filter the pump light. The flashlamp flow tube was Pyrex to attenuate the ultraviolet output of the lamp, which heats the laser rod without pumping the upper laser level. The flow tube enclosing the laser rod was samarium-doped glass, which absorbs at 1.06 μm.

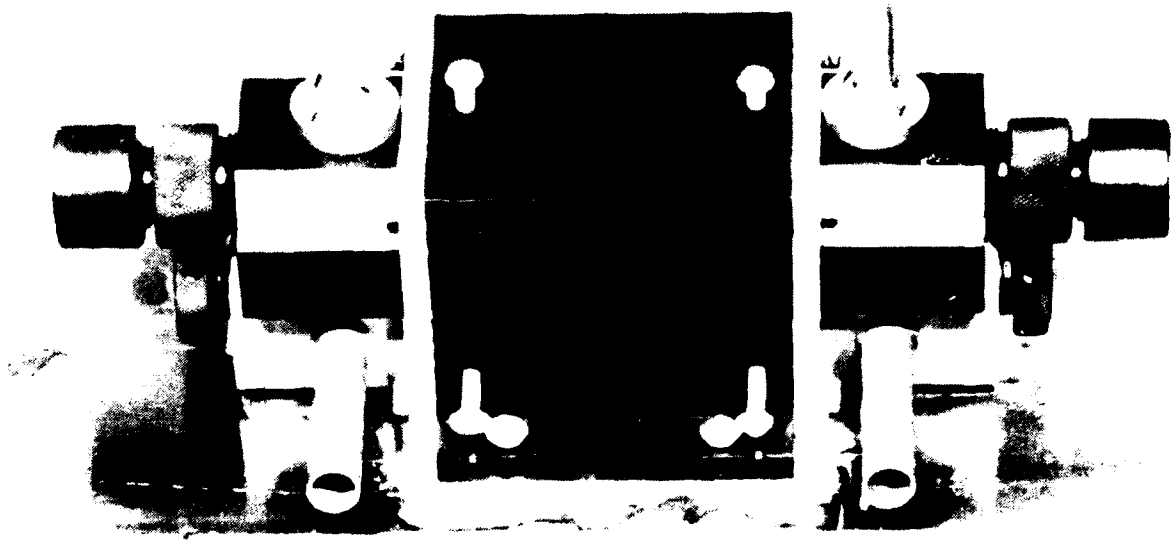

Figure 2.4. Low-Temperature Pump Cavity For 946 nm YAG Experiments

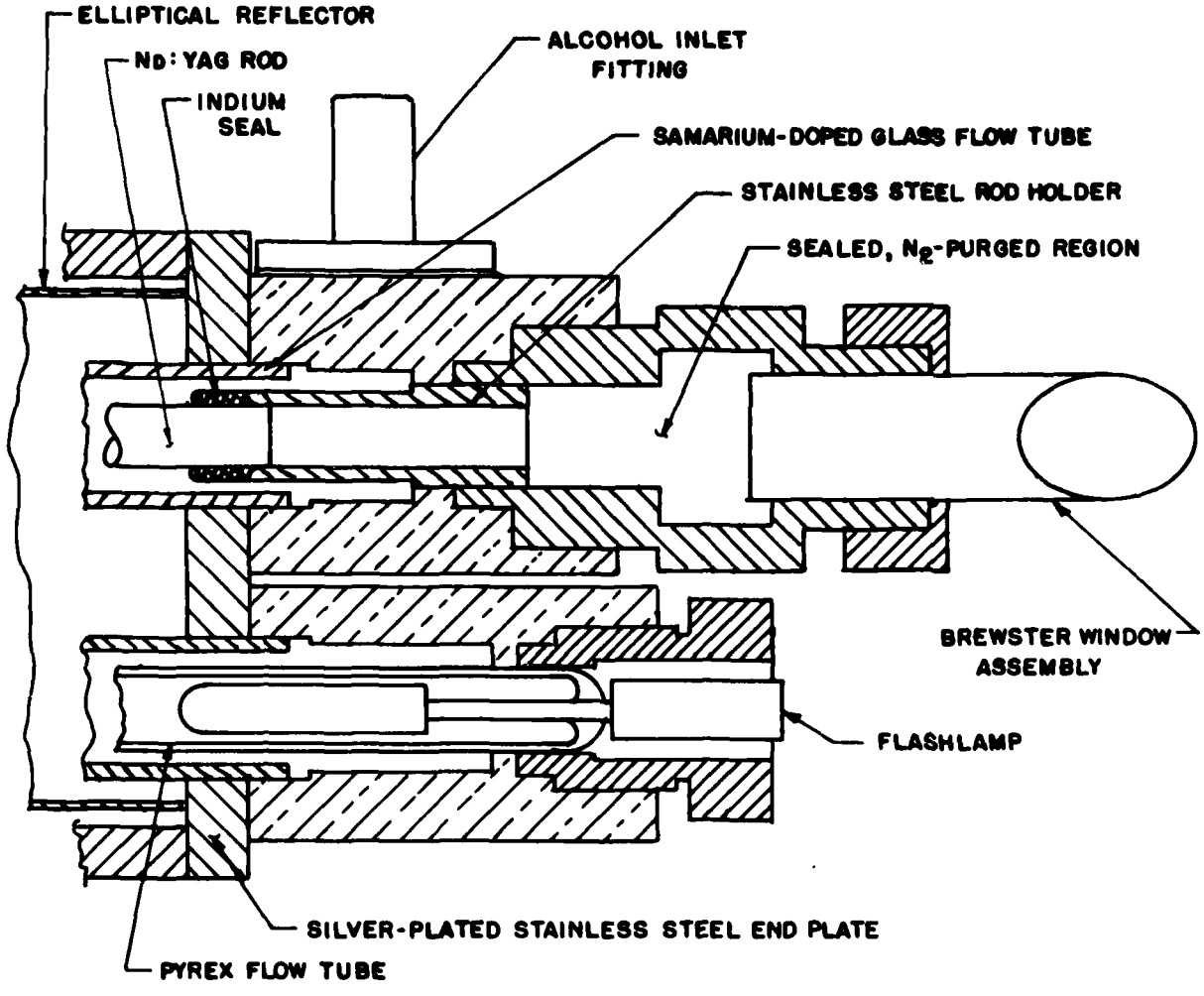

Figure 2.5. Low-Temperature Pump Cavity Assembly Detail

The absorption of samarium reduces the lateral depumping of the laser rod by attenuation the 1.06-μm component of flashlamp radiation, and by reducing the amount of spontaneously emitted 1.06 μm radiation which reflects from the pump cavity walls and returns to the rod.

Low-temperature operation of the laser rod presented unusual design problems. Thermal isolation between rod and flashlamp was provided by using materials with low thermal conductivity in the construction of the cavity. Stainless steel end plates and laser rod holders and Delrin mounting assemblies for the laser rod were used to minimize the flow of heat to the rod. The O-ring seals at the ends of the laser rod (see figure 2.5) presented difficulty because of the low temperatures at the rod. Silicone rubber O-rings typically leaked after a few cycles between room temperature and -60 C. Seals made from pure indium wire were more satisfactory, lasting for many temperature cycles if they survived the first one.[7] Pure indium wire is very soft, and can be formed easily into O-rings. Glass tubes with Brewster windows protected the ends of the laser rod from exposure to room air, to prevent water vapor condensation and frost. The volumes enclosed by these tubes were sealed, evacuated, and back-filled with dry nitrogen to remove water vapor.

The alcohol used to cool the laser rod was refrigerated and circulated by a Neslab model LT-9 cooling unit. This unit can regulate coolant temperatures between +10 C and -70 C (nominal). The alcohol flow rate through the pump cavity was 2.3 liters/minute (0.6 gallon/minute).

The flashlamp circuitry used to pump the rod consisted of an ILC-made 1500-torr krypton flashlamp with a bore diameter of 3 mm and a 2.5-inch arc length. The envelope was cerium-doped quartz, to reduce UV emission. The lamp was operated in simmer mode. The pulse forming network contained a 50-μF capacitor and a 23.5-μh inductor. The maximum energy attainable with our power supply was about 34 J. At this energy, the current pulse width was about 200 μsec at the 10% points.

The frequency-selective resonator design is shown in figure 2.6. Discrimination against lasing at 1.06 μm was provided by the dielectric coating on the resonator mirrors. Reflectances at 1.06 μm were typically 4%. The coatings were supplied by Broomer Research, Inc., of Plainview, NY, and by Laser Energy, Inc. of Rochester, NY. Additional discrimination against 1.06 μm was provided by the Brewster-angled dispersion prism, made of fused silica. The dispersion of fused silica introduces an angular deviation of 3.2 mrad per single pass between initially parallel rays of wavelength 1.06 μm and 946 nm. This introduces a 3.2-mrad difference between optimum mirror alignment at the two wavelengths. The only normal-incidence surfaces in the resonator (besides the mirrors) are the laser rod faces, which were anti-reflection coated at 1.06 μm with MgF. The coating is broad enough in wavelength that reflectance at 946 nm is also low, on the order of 0.5%. The use of Brewster-angle windows and dispersion prism polarizes the resonator and reduces the possibility of parasitic lasing. With careful alignment for operation at 946 nm, it was possible to prevent lasing at 1.06 μm at pumping energies up to 34 J.

Experimental Tests and Results

In the experimental studies, the pump cavity described previously was operated first as a 1.06-μm laser to establish a performance reference and to obtain 1.06-μm threshold data for estimation of the pumping rate K. The dispersion prism was added to the resonator, and 1.06-μm performance was checked again to evaluate its insertion loss. The 1.06-μm resonator mirrors were then replaced by the selective 946-nm mirrors. In operation at 946 nm, lasing threshold was measured as a function of temperature from 0 C to -63 C. When the pump cavity was operated as a 1.06 μm laser with mirror reflectances of 45% and 100%, threshold energy was 2.75 J. This energy leads to value of pumping constant K of 5.12×10^{16} ions/cm^3-joule for the R_2 component of $^4F_{3/2}$, and 9.07×10^{16} ions/cm^3-joule for the R_1 component at 210°C, as calculated in appendix I.A. Insertion of the Brewster prism increased the 1.06-μm threshold to 2.9 J.

Experimental measurements of 946 nm threshold are shown in figure 2.7. The pulse repetition frequency (PRF) was 2 Hz. The mirrors used in these

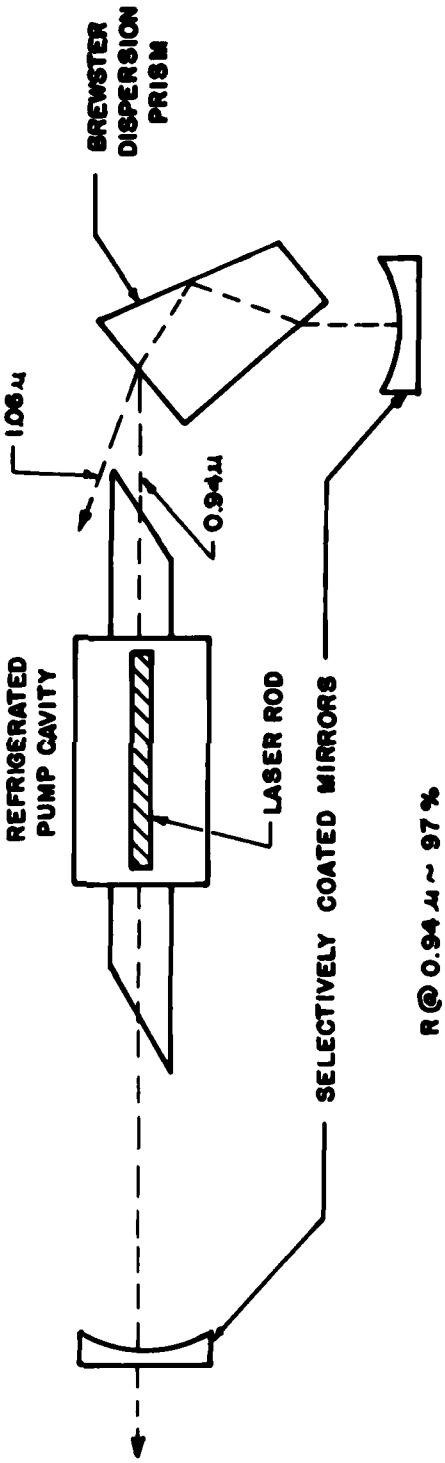

Figure 2.6. Frequency-Selective Resonator For 946 nm Nd^{+3} Testing

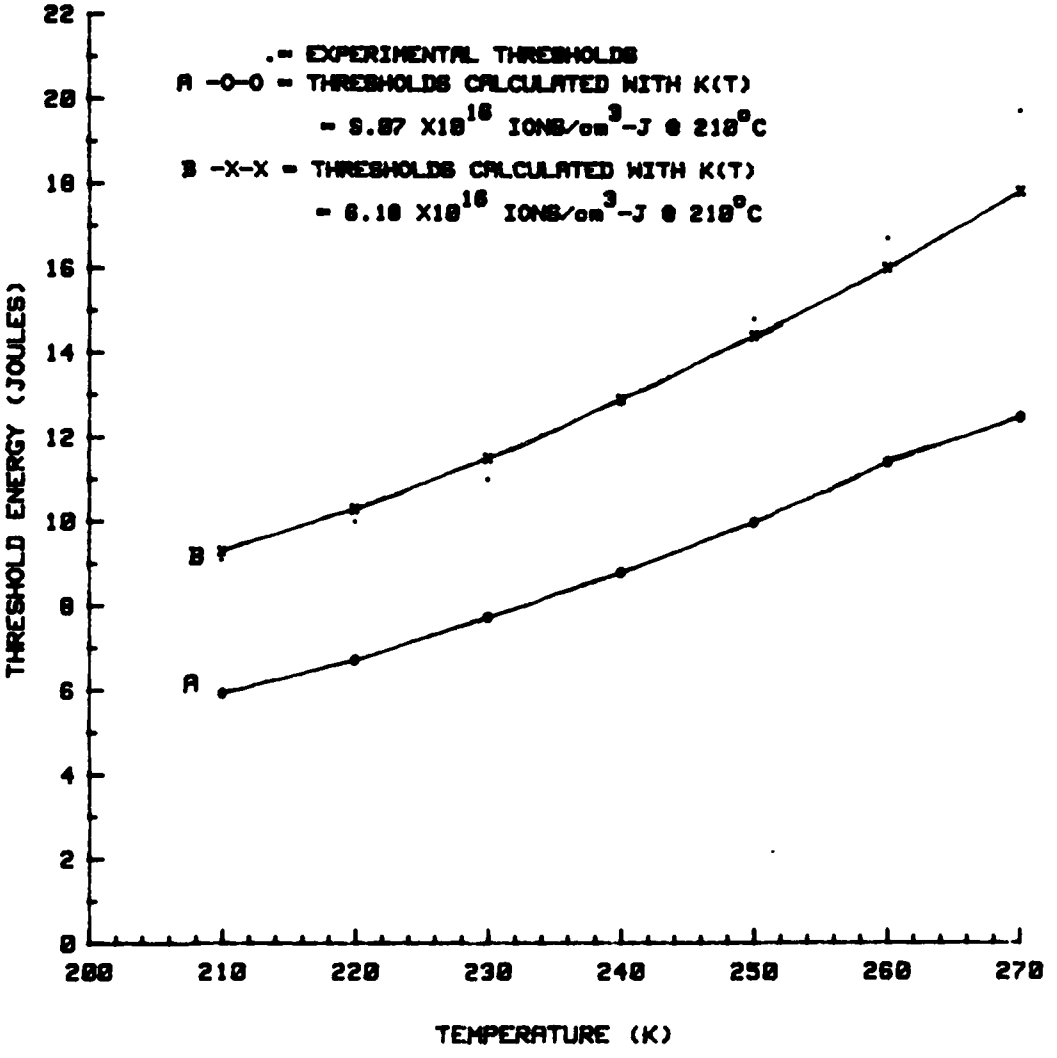

Figure 2.7. 946 nm Threshold Energy Versus Temperature

measurements had reflectances of 97.5% and 97.0% at 946 nm. Also plotted in figure 2.7 are theoretical thresholds calculated from the model described previously. The pumping constant K(T) in curve A was calculated from the 1.06 μm threshold as described in appendix I.A. The constant for curve B was determined by numerically fitting the experimental thresholds to the theoretical threshold inversions. Values of R = 0.946 and T_e = 0.94, appropriate for the experimental resonator, were used in the calculations.

In the measurement of output pulse energy at 946 nm, a dielectric polarizer was inserted in the resonator to provide a variable amount of output coupling (figure 2.8). The transmission of the polarizer for p-polarized 946-nm radiation is a function of incidence angle. At each above-threshold input energy, the incidence angle of the polarizer was adjusted to produce maximun power output. Total output power was measured as the sum of power coupled out in each reflection from the polarizer plus the amount emitted through the resonator mirrors, which transmitted about 3% of incident 946 nm radiation. As a consistency check, a resonator mirror with a 946-nm reflectance of 88% and a 1.06 μm reflectance of 79% was also used as an output coupler. Output energy measurements at a PRF of 2 Hz and a temperature of -63.5 C are shown in figure 2.9. Lasing at 1.06 μm was suppressed, but great care in alignment was necessary to do so. All the output energies obtained were considerably below the stored energy estimates of equation (2.5) and figure 2.3. The largest pulse energy obtained was 42 mJ observed with optimized output coupling provided by the dielectric polarizer.

After the measurements of 946-nm output energy, the pump cavity was again tested at 1.06 μm, using the same mirrors and configuration used in the initial 1.06 μm performance test. A 1.06-μm threshold of 3.9 J was obtained, for comparison with the 2.75 J threshold observed previously. A long-pulse output energy of 270 mJ was measured for a capacitor energy of 34.2 J. Slope efficiency was 0.98%.

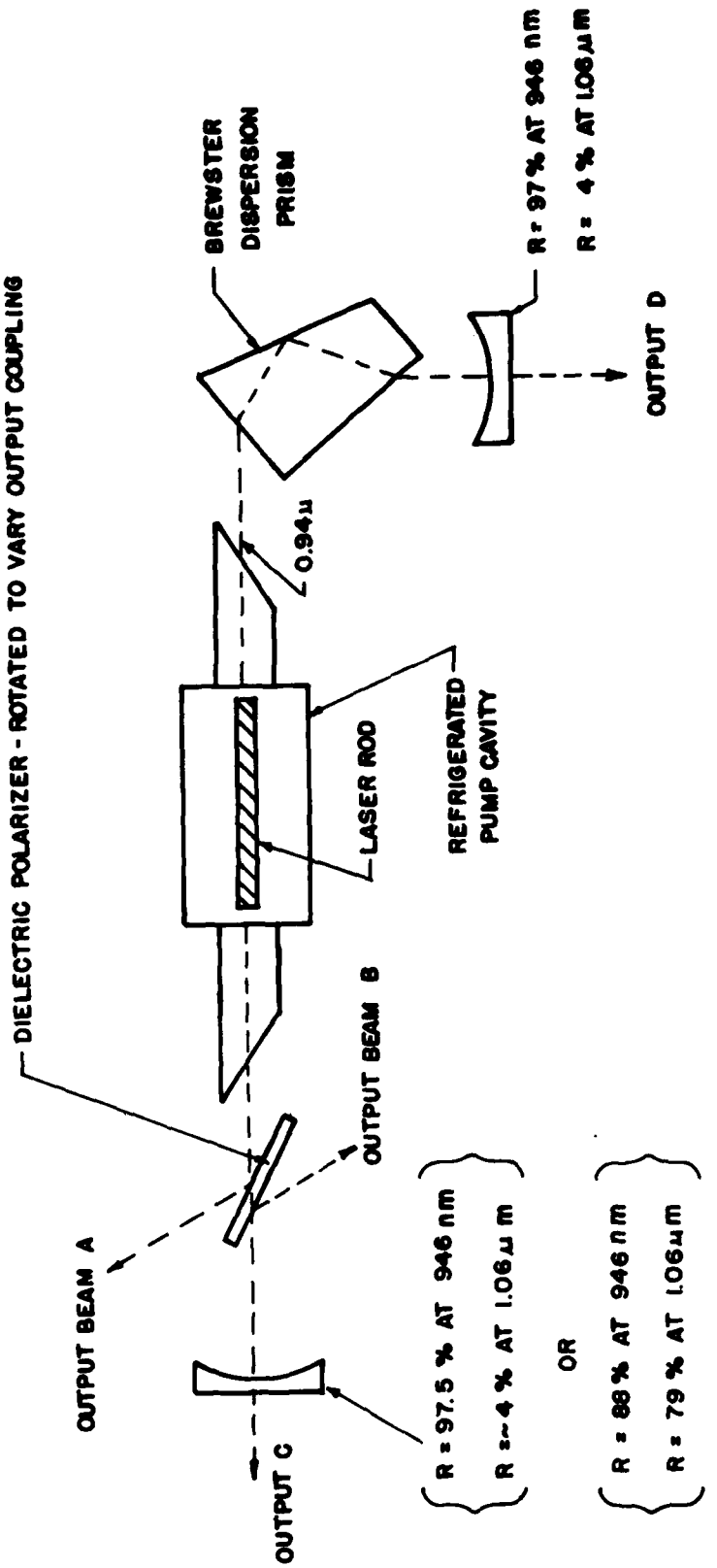

Figure 2.8. Resonator Configuration For 946 nm Output Coupling Tests

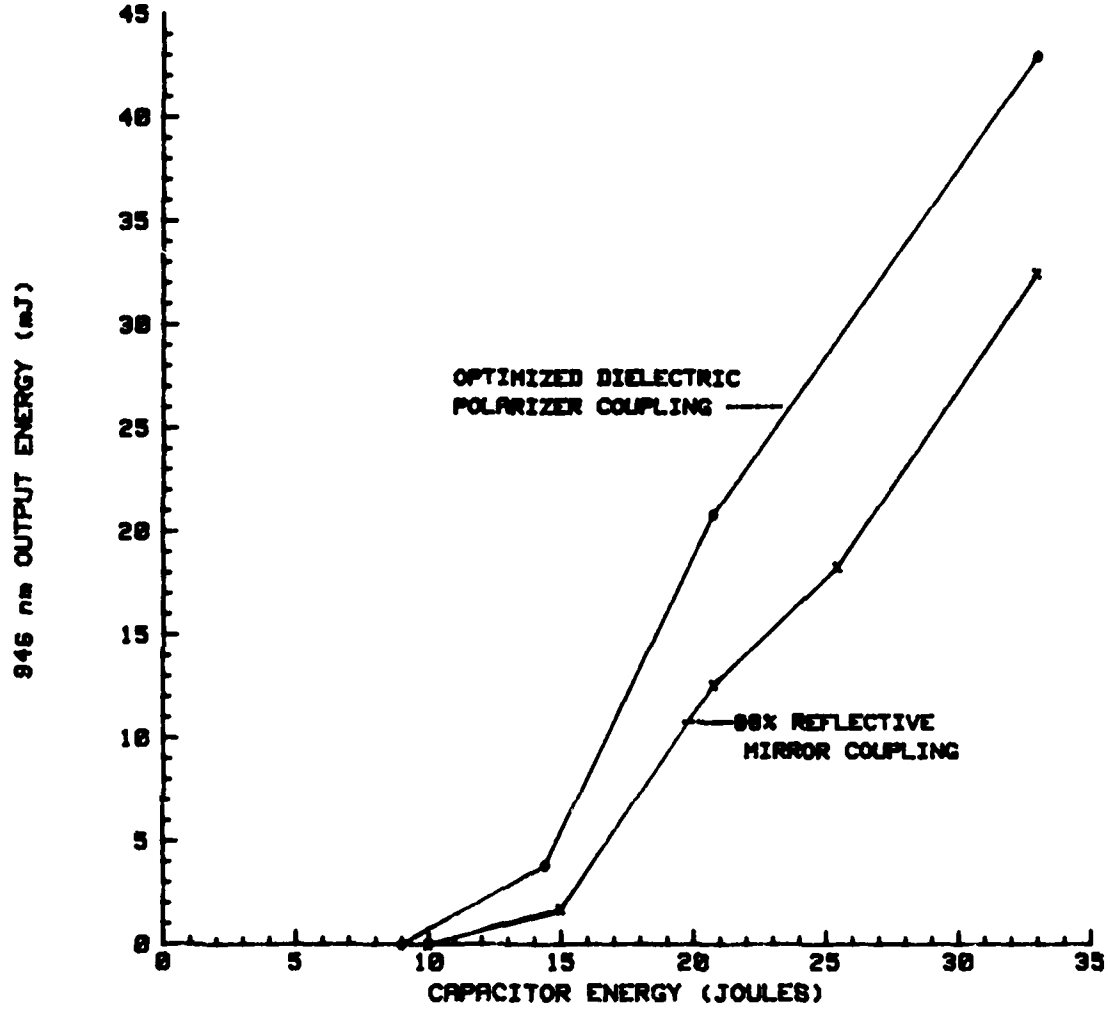

Figure 2.9. 946 nm Output Energy At -63.5 C (210°K)

Measurements were then made of the spontaneous fluorescence at 1.06 μm and 946 nm emitted by the pumped laser rod in the low-temperature pumped cavity. No resonator mirrors were used during this measurement. Fluoresence was detected with an S-1 photomultiplier made by EG&G (model 585-63). Interference filters were used to isolate the two fluorescence wavelengths. The pump energies covered the range of energy used in the lasing tests. Figure 2.10a shows the peak fluoresence intensity at 946 nm and at 1.06 μm. Figure 2.10b gives their ratio plotted against capacitor energy. The intensity measurements are not corrected for detector and filter response at each wavelength and are therefore relative measurements. The fluorescence pulses were photographed on an oscilloscope, and the decay of fluorescence intensity was measured and fitted to an exponential decay of the form $I(t) = I_0 \exp(-t/\tau)$. The decay times τ determined from these fits are plotted against flashlamp energy in figure 2.10c.

Discussion of Results

The experimental thresholds for the 946-nm transition agree surprisingly well with thresholds predicted by the model, provided a suitable value is chosen for the pumping constant K(T). The initial value, K(210 K) = 9.07 x 10^{16} ions/cm^3-joule, estimated from a 1.06-μm threshold of 2.75 J, predicts thresholds low by 3.8 to 7.2 J over the temperature range. Better agreement results from using K = 6.18 x 10^{16} ions/cm^3-joule, determined by assuming resonator losses of 6% per single pass and fitting the pump rate to the experimental points. The remaining difference could be due to an overestimation of the resonator loss, which is not temperature-dependent, or to temperature-dependent effects not included in the model. The remeasurement of the 1.06-μm performance after the 946-nm experiments yielded a threshold of 3.9 J. This threshold predicts a value K(210 K) = 6.39 x 10^{16} ions/cm^3-joule, close to the value fitted to the data. Part of this change in pumping efficiency may be due to the replacement of the flashlamp during the experiments, and part may result from deterioration of the pump cavity reflector due to ultraviolet irradiation from the flashlamp. The agreement between the experimental

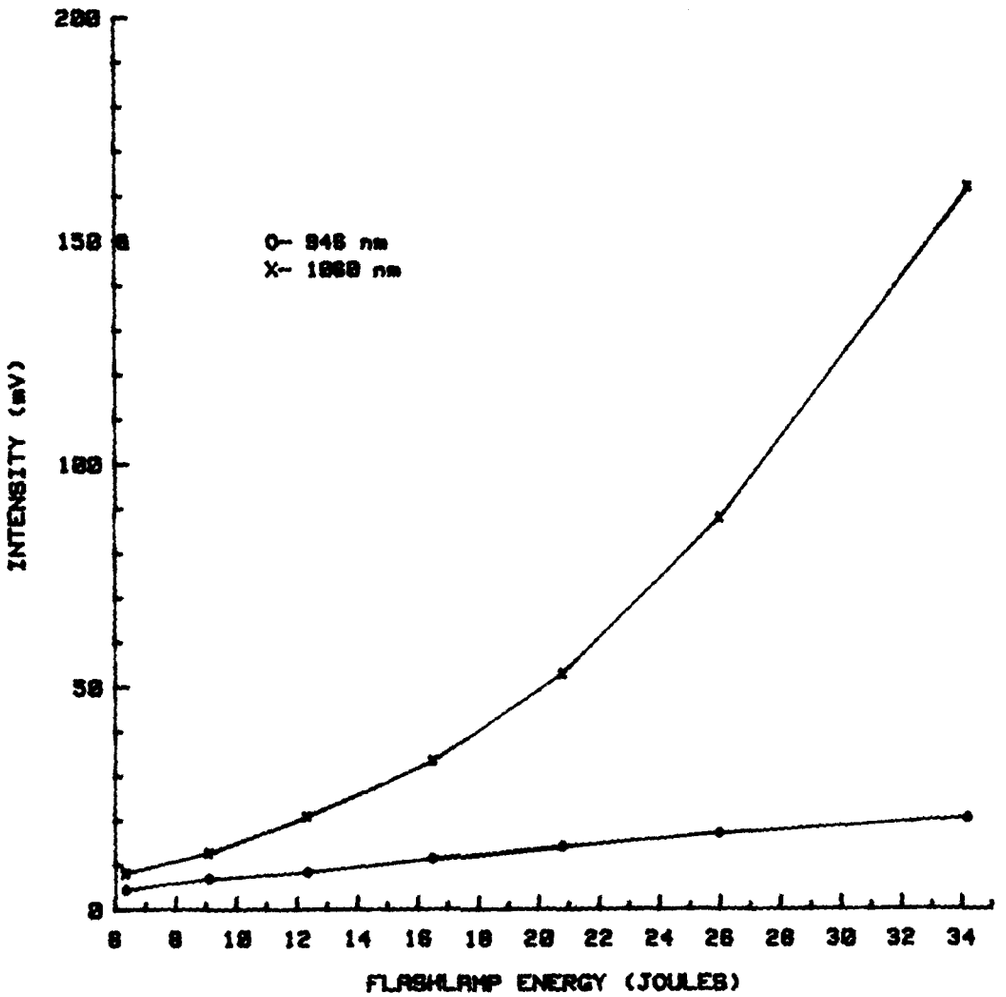

Figure 2.10a. Spontaneous Emission Results At 946 nm And 1060 nm

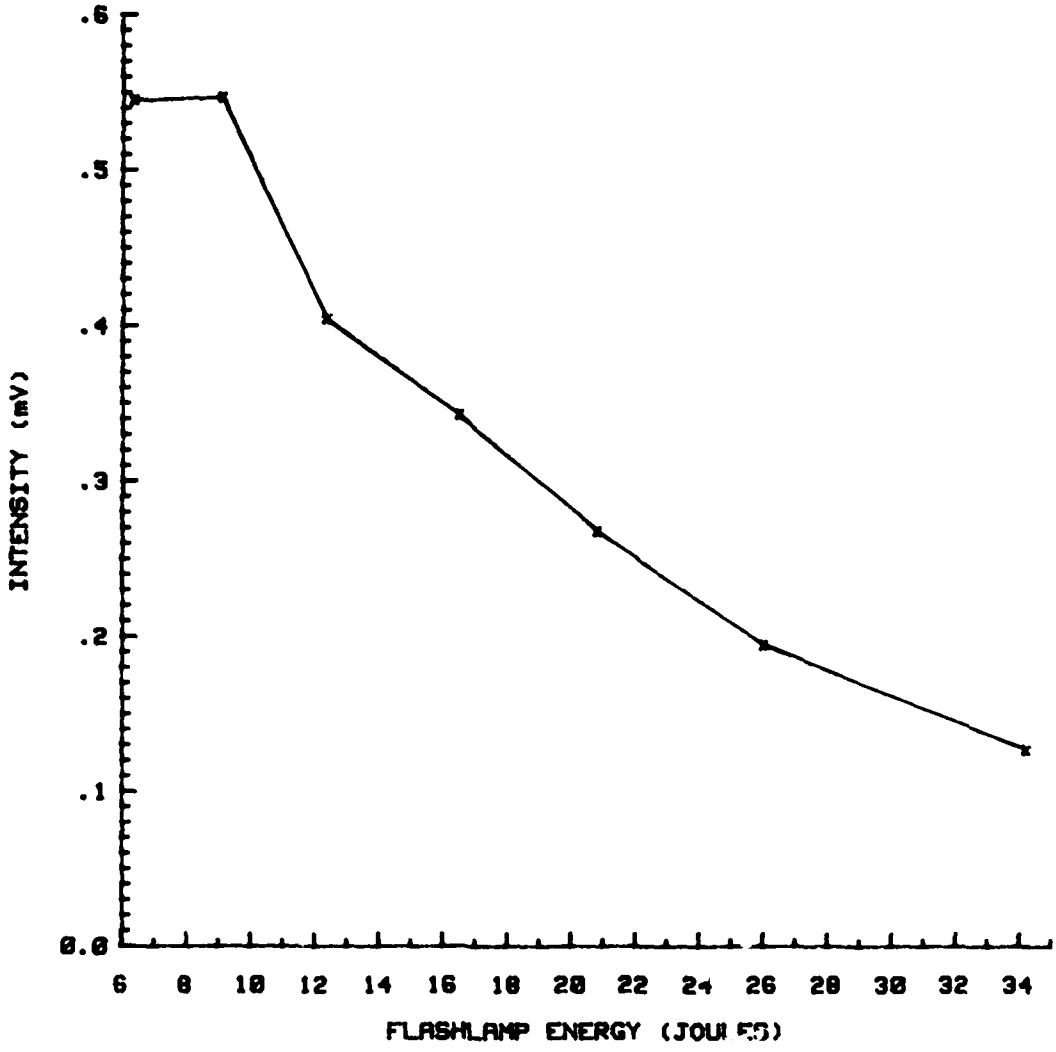

Figure 2.10b. I_{946}/I_{1060} Versus Flashlamp Energy

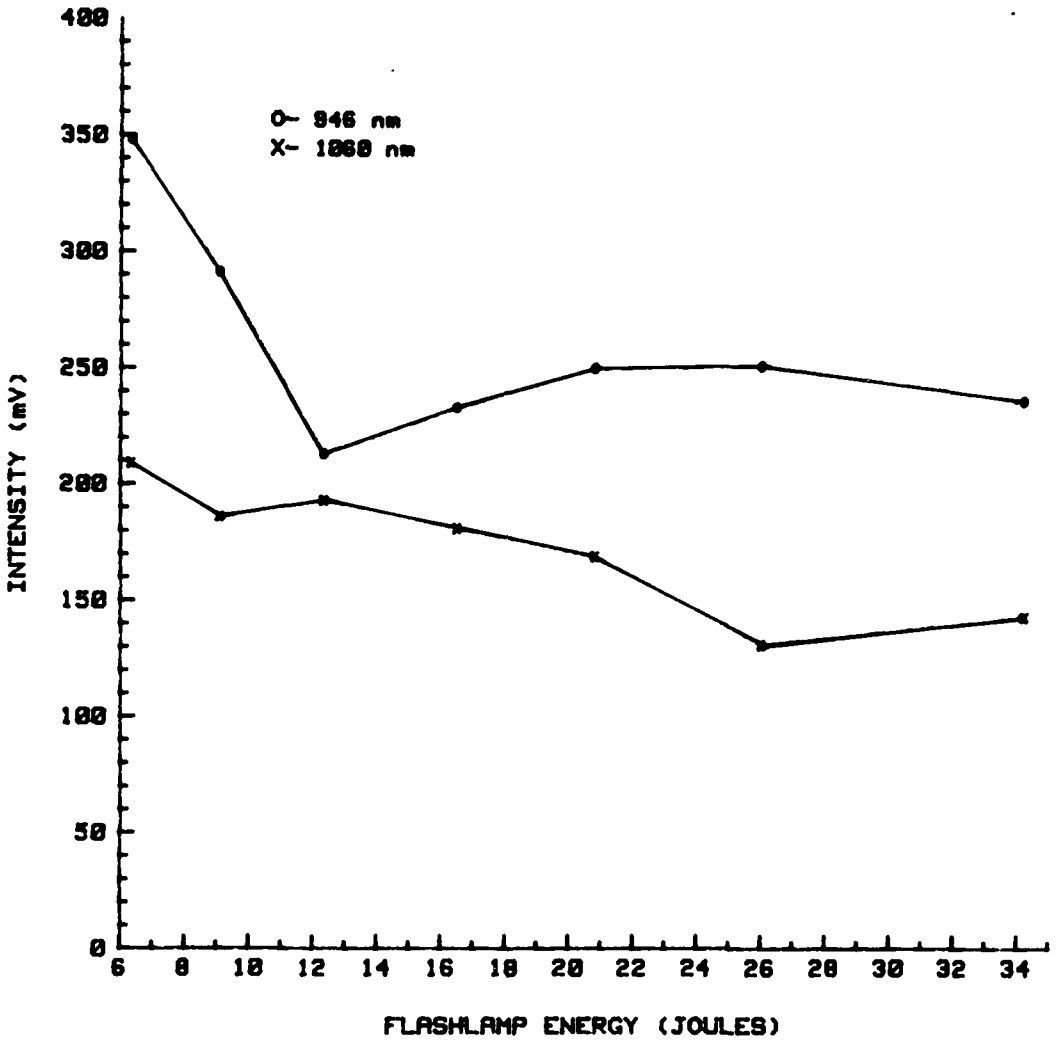

Figure 2.10c. Decay Time Constant Versus Flashlamp Energy

thresholds and the revised pumping constant may be somewhat fortuitous, but it lends a degree of confidence to the model, and to the estimates of the pumping constant K(T) and resonator losses.

The output pulse energy measurements present a less satisfactory picture. The final lasing measurements at 1.06 μm gave a slope efficiency of 0.98%. If the same number of photons can be extracted at 946 nm, a slope efficiency of 1.1% would be expected based on the photon energy ratio. Pumping the rod to 22 J above the 946-nm threshold (the largest pumping achieved experimentally) should produce about 240 mJ of stored energy. Experimentally, we obtained 42 mJ under these conditions, with the output coupling optimized. Optimum output coupling for the 946-nm transition is smaller than for the 1.06-μm transition because of the difference in gain, and more efficient energy extraction occurs with larger values of optimum coupling, assuming fixed passive losses. For the conditions under discussion here, coupling efficiency could account for some 10% of the energy loss. However, some 174 mJ of inversion energy remains unextracted at 946 nm.

The spontaneous emission measurements shown in figure 2.10 give some indication of conditions in the pumped rod. The 946-nm peak fluorescence increases linearly with flashlamp energy, while the 1.06-μm fluorescence increases quadratically with energy. The decay lifetime of the 1.06-μm fluorescence is smaller than the 230-μ fluorescent lifetime of the $^4F_{3/2}$ level, and appears to diminish slightly as pump energy increases. The lifetime of the 946-nm fluorescence is larger than 230 μsec, and shows a rather uncertain dependence on pump energy. In both cases, the low-energy lifetimes may be influenced by the tail of the pumping pulse. These results suggest the occurrence of amplified spontaneous emission (ASE) at 1.06 μm. The quadratic fluorescence growth and shorter fluorescence lifetimes at 1.06 μm are both consistent with ASE. However, the linearity of the 946-nm peak fluorescence data and the larger value of its decay lifetime seem inconsistent, since the upper levels for the two transitions are so closely coupled. One possible explanation is that the ASE at 1.06 μm is not strong enough to deplete the $^4F_{3/2}$ population significantly. The 946-nm emission would then provide a reliable measure of the upper level population. This interpretation doesn't explain the different values of fluorescence decay lifetime. A second interpretation

suggests that the 1.06-μm ASE is indeed depleting the population, but that its effects on the 946-nm fluorescence are masked, possibly by pumping in the "tail" of the flashlamp pulse. The weaker 946-nm fluorescence signal would be more vulnerable to any interfering process.

Two explanations for the low 946-nm lasing output energy are consistent with these results. One is that 1.06-μm ASE depletes population of the $^4F_{3/2}$ level, and reduces the inversion energy available for 946 nm lasing. Alternately, ASE may not be significant, and another explanation is necessary. Excited state absorption at 946 nm from the $^4F_{3/2}$ level to another level 10,570.8 cm^{-1} above the $^4F_{3/2}$ could occur. In threshold calculations, the cross-section for excited state absorption should be subtracted from the stimulated emission cross-section to obtain a smaller effective value of cross-section, leading to larger threshold energies than those obtained with the true cross-section. The threshold measurements of figure 2.7 can be interpreted in this way. If the discrepancy between the theoretical thresholds of curve A and the experimental thresholds is attributed to excited state absorption, one could deduce an effective stimulated emission cross-section of 3.4×10^{-20} cm^2 from the ratio of theoretical to experimental thresholds, which averages 0.669. Atributing the 33% reduction in cross-section to excited state absorption leads to an absorption cross-section of 1.68×10^{-20} cm^2 for the postulated process.

In summary, our lower than expected pulse energies can be interpreted as either due to amplified spontaneous emission at 1.06 μm or to excited state absorption at 946 nm. Both processes provide channels for the inversion energy which compete with the 946-nm lasing process.

SECTION 3

$LiHoF_4$ LASING STUDIES AT 979 nm

$LiHoF_4$ is one member of a large class of solid state lasing materials called rare-earth fluorides. In these materials, the host lattice is $LiYF_4$ (often called YLF), and the active (lasing) rare earth ion is substituted at the yttrium site in the crystal structure. The transition of interest for this project was the $^5F_5 \rightarrow {}^5I_7$ transition in Ho^{+3}, with a wavelength of 979 nm. The transition is a 4-level type at room temperature. The second harmonic of the transition wavelength, 489.5 nm, matches quite well the optimum transmission wavelength for deep oceanic waters. Holmium-doped $LiYF_4$ is unusual in that Ho can be substituted at the yttrium sites in any amount, from trace (usually denoted Ho:$LiYF_4$ or Ho:YLF) to 100% substitution, yielding $LiHoF_4$. Reports in the Russian literature in 1975 and 1976 described lasing of $LiHoF_4$ at 979 nm with thresholds of $\sim$ 7.5 J,[8] and 2% Ho:$LiYF_4$ with thresholds of $\sim$ 13.5 J.[9] Further discussions with personnel at Sanders Associates and MIT raised the possibility of operation at higher temperatures, through refinements in growth technique and the use of a different crystal orientation. The material was therefore considered to have the possibility of lasing near room temperature in a 4-level energy structure. The possibility of a near-room temperature, 4-level solid state laser with a useful wavelength was attractive, and a boule of $LiHoF_4$ was grown by Sanders Associates. The boule yielded four laser rods: two were 25 mm long, two were 76 mm long, and all had diameters of 5 mm. The rod faces were anti-reflection coated for 979 nm.

Spectroscopic studies[10] at the CPOEL of MIT produced significant new information about $LiHoF_4$. The fluorescent lifetime of the upper laser level $^5F_5$ was found to be 16 μs at 300 K, and increased to 33 μs at 77 K. The stimulated emission cross-section at 300 K was 4×10^{-20} cm^2. At 77 K it was 2×10^{-19} cm^2. The lifetime of the terminal level $^5I_7$ was 15 ms at both temperatures. The energy level structure is shown in figure 3.1.

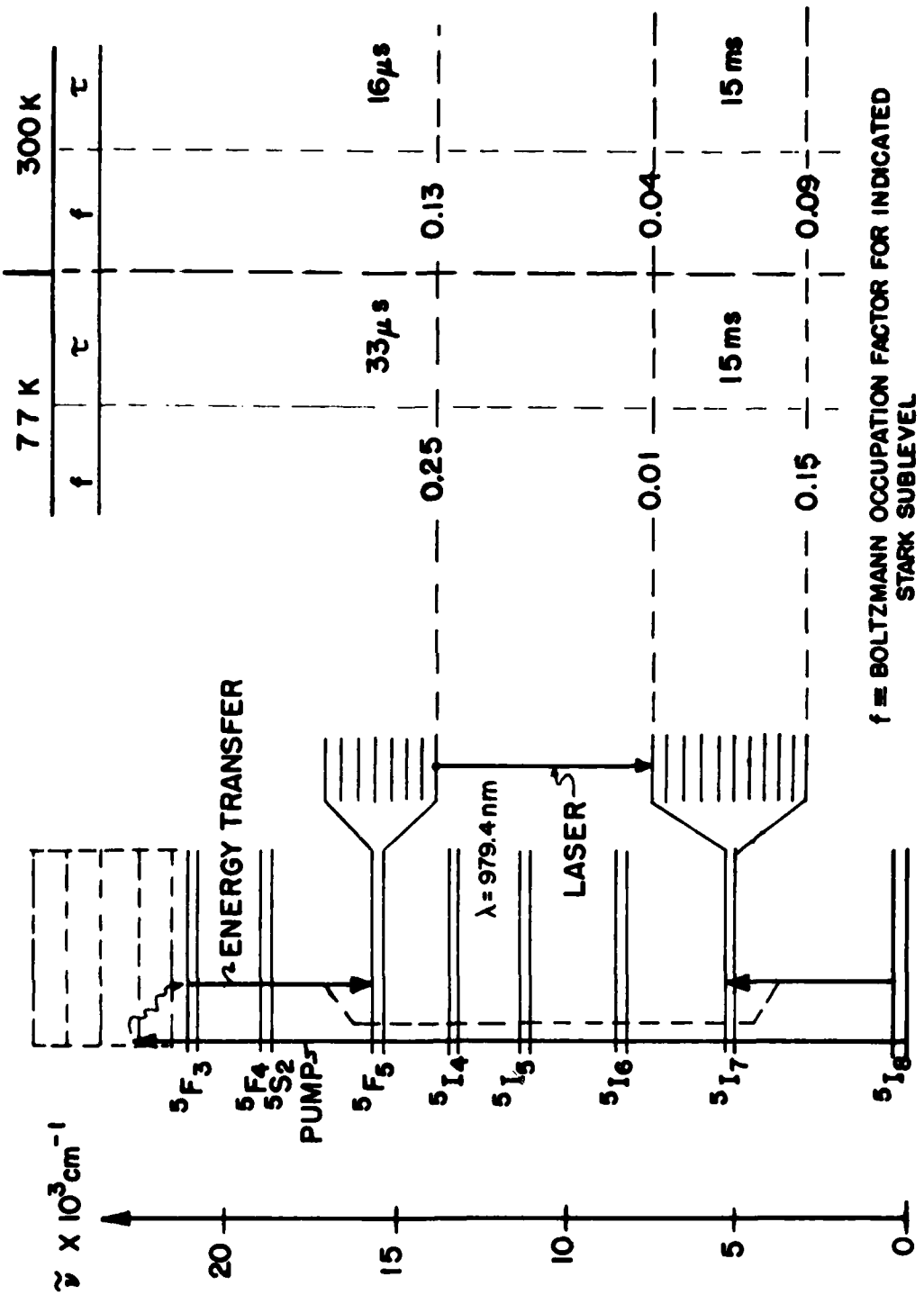

Figure 3.1. Li Ho F^4 Energy Levels

A most significant feature of the process of pumping the $^5F_5$ level was the resonance shown in figure 3.1, in which relaxation of an excited Ho ion from the pump bands to the $^5F_5$ level occurred by energy transfer to another unexcited Ho ion, raising the second ion to the $^5I_7$ level. This "resonant" energy transfer pumps the lower level as effectively as the upper, and greatly reduces the inversion attainable between the two levels. Inversion is still possible in this situation because of the existence of Stark-split sublevels of both $^5F_5$ and $^5I_7$ levels. Population of each of these sublevels is determined by the Boltzmann distribution. Inversion can occur between the most populated (lowest) sublevel of $^5F_5$ and the least populated (highest) sublevel of $^5I_7$. The small-signal gain is reduced, however, because only a fraction of the total population of $^5F_5$ is inverted with respect to $^5I_7$. Numerically, the effect on small signal gain is given by:

$$g = (f_u - f_l)\ \sigma\ N \tag{3.1}$$

in which

g = small-signal gain coefficient [cm^{-1}]

f_u = occupation factor for the lowest Stark sublevel of the $^5F_5$ manifold [dimensionless]

f_l = occupation factor for the highest sublevel of the $^5I_7$ manifold [dimensionless]

σ = stimulated emission cross-section [cm^2]

N = density of Ho ions in $^5F_5$ and $^5I_7$ levels, assumed identical due to resonance [cm^{-3}]

Limited estimates of performance for $LiHoF_4$ can be deduced from the above information. The fluorescent lifetime of the upper level is short ($\leq$ 33 μs) relative to the flashlamp pulse durations required for long-life lamp operation. Crude estimates of lasing threshold ranged from a lower bound of 50 J to an upper bound of 600 J. The combination of high threshold and limited energy storage reduces the practicality of $LiHoF_4$ for naval applications.

Experimental Testing

Lasing experiments were conducted with $LiHoF_4$ to test the tentative conclusions discussed above. The low-temperature apparatus and flashlamp circuitry developed for the Nd:YAG testing were modified for $LiHoF_4$. Tests were conducted at the lowest accessible temperature, -63.5° C.

The low-temperature pump cavity described in section 2 was rebuilt to increase its pumping efficiency in the visible and near ultraviolet, matching the pump bands of $LiHoF_4$. The elliptical quartz reflector was replaced by an aluminum clamshell reflector overcoated with evaporated aluminum for maximum ultraviolet reflectance. Nitrogen purging was added to prevent frost accumulation. Pyrex and samarium flow tubes were replaced by fused silica, and flashlamps with natural or synthetic fused silica envelopes were used to minimize ultraviolet absorption. The flashlamps had 3-mm bore diameters, 6.35-cm (2.5-in) arc length, and were filled with xenon at 1500 torr. The modified pump cavity is shown in figure 3.2.

The driving circuitry for the flashlamp was redesigned to produce shorter current pulse widths, to match more closely the fluorescent lifetime of $LiHoF_4$. Figure 3.3 shows the circuit used. At discharge energies of about 50 J, the circuit generated a current pulse with a width of 32 μs and a peak current of 2024 A. Parallel triggering of the lamp in this circuit led to breakage after 20 to 30 shots typically. Simmering the lamp at a current of 100 mA eliminated this problem.

The resonator for the experiment is also shown in figure 3.3. Two concave reflectors with 10-meter radii of curvature coated for maximum reflectance at 979 nm were placed symmetrically about the pump cavity, spaced apart by 30 cm. Mirror alignment required a white light autocollimator, as $LiHoF_4$ absorbs strongly at 632.8 nm.

Lasing was not obtained with this apparatus, and it was concluded that threshold energy exceeded 51.25 J, the limit available from the power supply. This negative result is consistent with the estimates of threshold energy discussed earlier. No further study of $LiHoF_4$ is planned at this time.

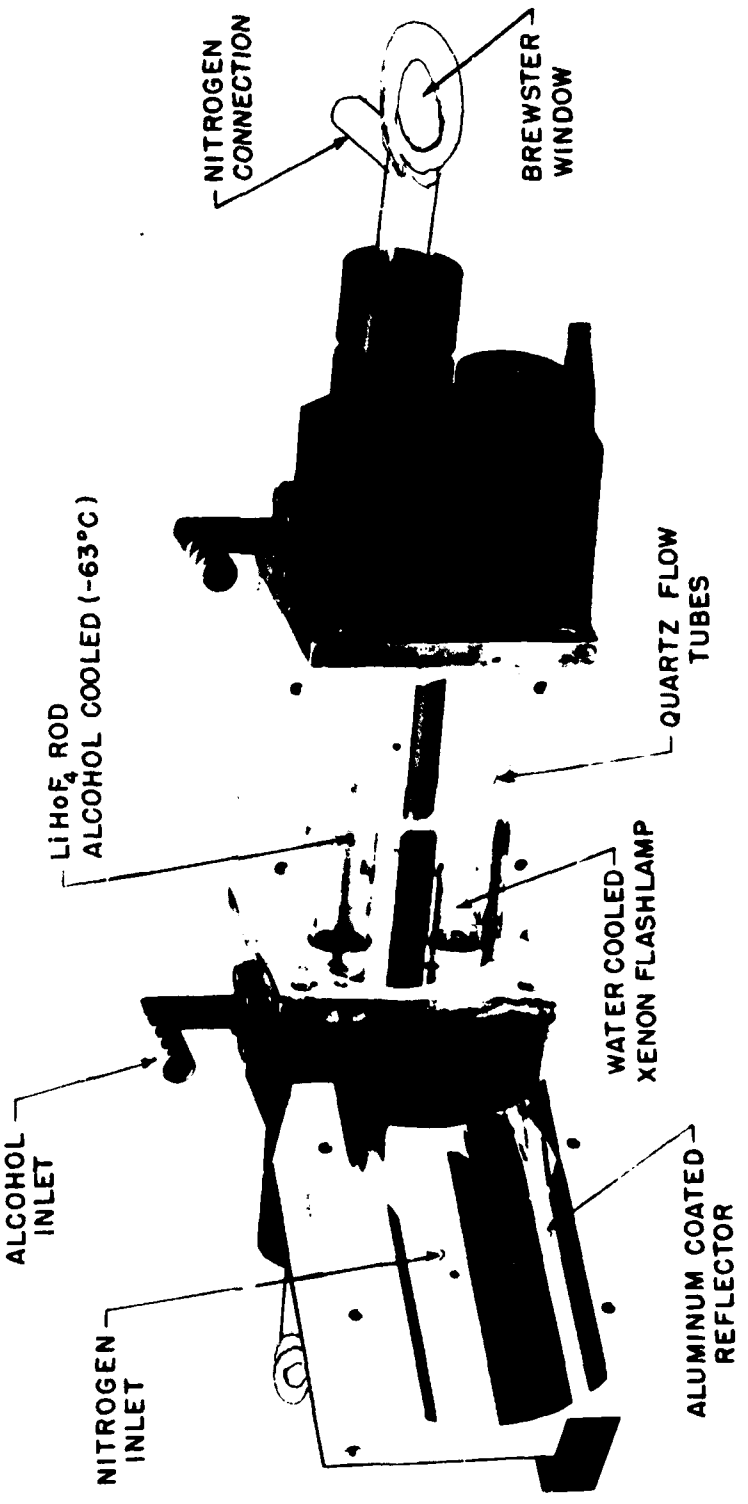

Figure 3.2. Li Ho F^4 Laser Pump Cavity

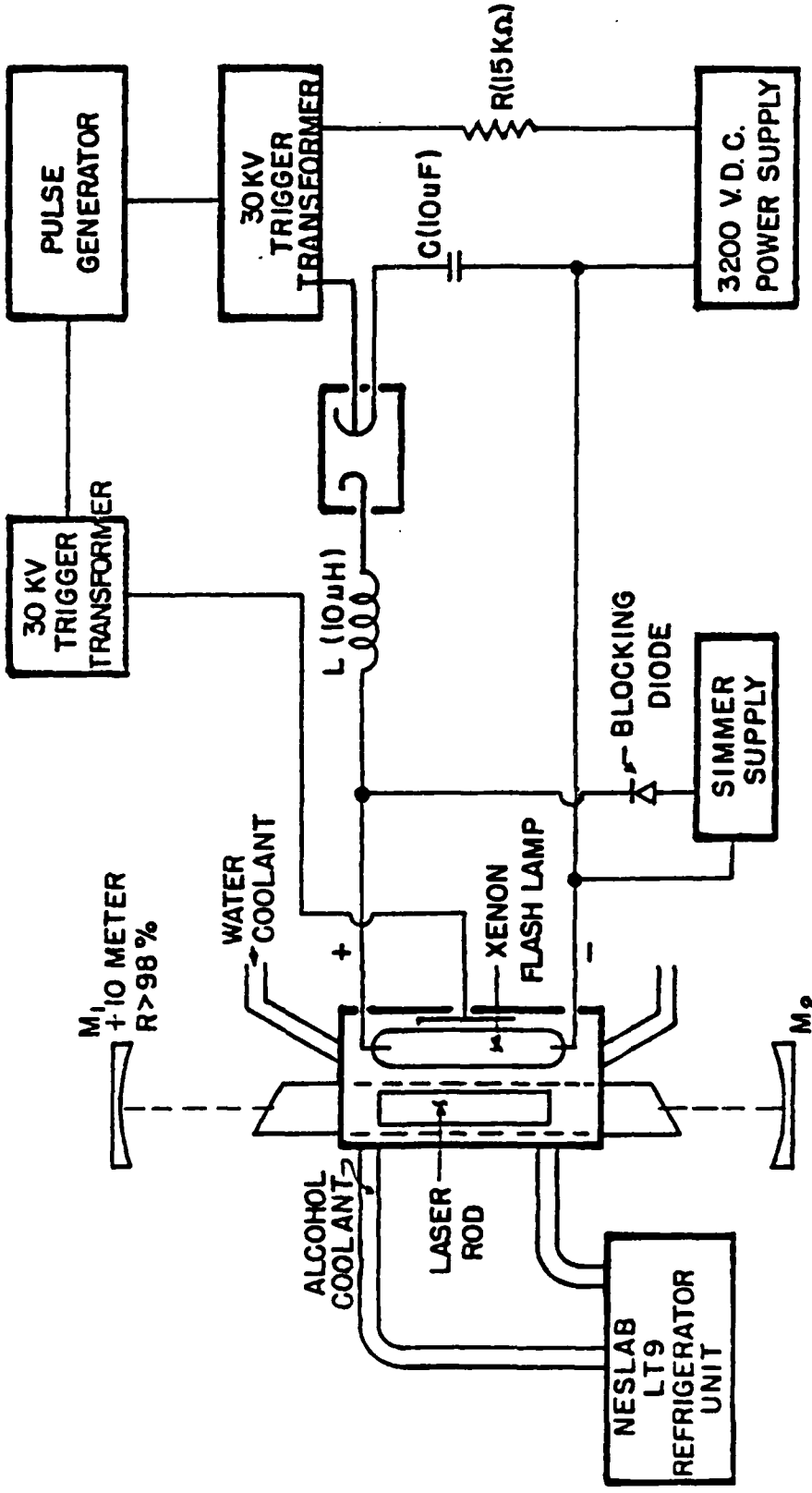

Figure 3.3. Li Ho F^4, 949 nm Experimental Breadboard Laser

SECTION 4

$LiTbF_4$, Er:$LiYF_4$ AND THE EFFICIENCY OF REFRIGERATED LASER MATERIALS

$LiTbF_4$ and Er:$LiYF_4$ were proposed as potential green-emitting solid-state laser materials, lasing at 545 and 550 nm, respectively. The materials were grown and studied spectroscopically at MIT in the CPOEL. Low temperature operation near 77 K was anticipated as necessary for the efficient operation of these materials. This section describes the properties of each material relating to the lasing transitions, the results of the investigations at MIT, and a first-order analysis of the impact of refrigerated operation on the efficiency of solid-state materials.

$LiTbF_4$ - $LiTbF_4$ was studied to assess its practicality as a 4-level laser material emitting at 545 nm. The point of departure for the study was an investigation[11] at the MIT Crystal Physics Laboratory in 1971-1973 in which terbium-doped rare-earth fluorides were grown, and spectroscopy and lasing measurements conducted. A sample of Tb:$LiGdF_4$ was lased at room temperature at 545 nm, with a threshold of 75 J. The sample produced 50 mJ of output energy at a flashlamp input energy of 150 J. The stimulated emission coefficient for the 545 nm transition was estimated as $5 \pm 2 \times 10^{-21}$ cm^2 at room temperature.

Reference [11] suggested several ways to improve terbium-doped rare-earth fluorides, and these were explored in the present project. The use of higher-purity materials and new growth technology were expected to improve the optical quality and the attainable size of crystals. In view of the small lasing cross-section, large active ion densities were suggested to increase the gain. The crystal $LiTbF_4$ was suggested as one in which the desirable Tb lasing properties would be preserved at high Tb densities (10^{22} cm^{-3}). Cooling the material from room temperature to 77 K was expected to increase the stimulated emission coefficient by a factor of 10. Finally, the use of the longest possible crystal length would increase the single-pass gain of the material, further reducing the threshold for lasing. The sum total of these suggestions was the consideration of a 10-cm long by 5-mm diameter rod of $LiTbF_4$ pumped by a xenon flashlamp and operated at temperatures as low as 77 K. Under the

joint ONR-NAVAIRDEVCEN program, the group at MIT undertook the growth of $LiTbF_4$ and its spectroscopic evaluation at room temperature and at 77 K. The temperature dependence of the stimulated emission coefficient had not been measured at the time.

Figure 4.1 shows the energy level structure of Tb-doped $LiYF_4$. The pump bands for the upper laser level $^5D_4$ fall in the 25,000 cm^{-1}-40,000 cm^{-1} region. The quantum efficiency of excitation of the $^5D_4$ level is believed to be close to 100%, meaning that all the energy actually absorbed in the pump bands produces $^5D_4$ population. The wavelength range of the pump bands, 250 to 400 nm, matches well the spectral emission of a xenon flashlamp with peak current density of 2500 A/cm^2 or more.[12] Efficient pumping of the upper laser level appeared possible with xenon lamps. The fluorescent lifetime of the $^5D_4$ level was known[11] to be about 5 ms and independent of the concentration of Tb in $LiYF_4$ up to 25% substitution. These factors, together with the 4-level nature of the transition, suggested that efficient lasing would be possible in $LiTbF_4$ if threshold could be attained at reasonable flashlamp energies.

Lasing performance estimates were made at NAVAIRDEVCEN. An attempt was made to estimate the lasing threshold and slope efficiency of the "optimum" terbium material described above, using the experimental results described in reference [11]. The expected temperature dependence of the stimulated emission coefficient was incorporated. Pulsed and CW operation were both considered, with xenon flashlamps as pump sources. The results of the performance estimates are shown in table 4.1.

TABLE 4.1

$LiTbF_4$ PERFORMANCE ESTIMATES

T [K]	σ [cm^2]	Pulsed Threshold [J]	CW Threshold [W]
77	5×10^{-20}	3.05	1.52×10^{3}
300	5×10^{-21}	30.5	$1.52 \times 10^{+4}$

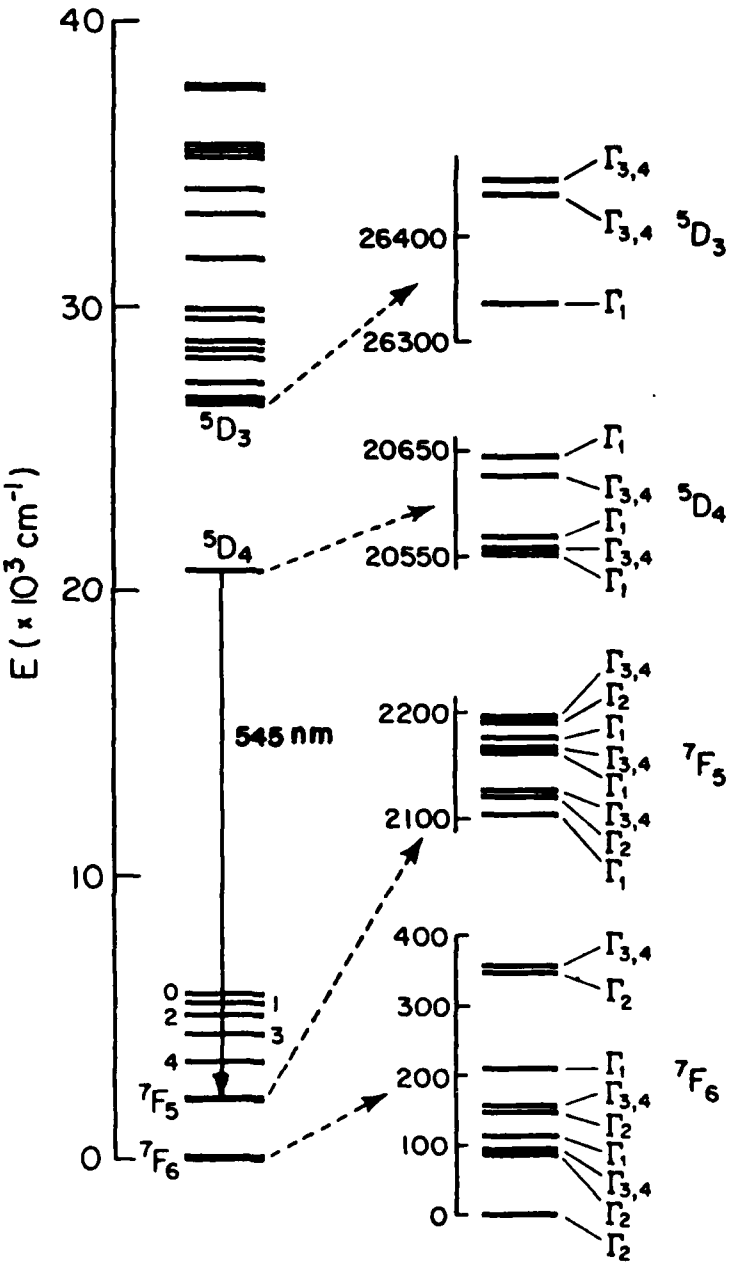

Figure 4.1. Tb^{+3} Energy Levels

The slope efficiency was estimated at 3%. These estimates were known to be very approximate, but the results associated with the cross-section of 5 X 10^{-20} cm^2 were quite interesting, and compared well with those of ND:YAG at 1.06 μm.

Crystals of $LiTbF_4$ were grown at MIT, and spectroscopy studies were performed on samples from the growth. Laser-quality material proved elusive. Most of the samples contained scattering centers, believed to be Tb_2O_3 particles resulting from oxygen contamination of the cover gas in the growth furnace. At least one pulling of an initially clear boule "went bad," developing dislocations and multiple-crystal structure for reasons not understood. It was not possible to grow a scatter-free boule large enough to yield a 10 cm long laser rod.

The spectroscopy results were similarly disappointing. The room temperature σ was measured to be 1.06 X 10^{-21} cm^2, a factor of 5 smaller than previous measurements in $Tb:LtGdF_4$.[13] At 77 K, the cross-section increased to $1.6x10^{-21}$ cm^2. A factor-of-10 increase relative to room temperature had been expected, and it was not clear why this was not observed. One possibility was the incomplete separation of polarizations in the measurement. The most crucial implication of this cross-section is a high threshold for lasing, compared to the estimates in table 4.1.

Er:$LiYF_4$ - This material was studied by the MIT group as a second possible green-emitting solid-state laser material. The practicality of operation at liquid nitrogen temperatures, around 77 K, was assumed in order to focus on the intrinsic potential of the material under most favorable conditions of operation. The transition considered was the $^4S_{3/2} \rightarrow {}^4I_{15/2}$ transition at 550 nm, shown in figure 4.2.

At the outset, information about this transition was limited. Some knowledge of the pumping processes was available from previous studies of the related transition, $^4S_{3/2} \rightarrow {}^4I_{13/2}$ at 850 nm.[14] Since this transition employs the same upper level, experience with it could be applied to the 550-nm transition. However, the stimulated emission cross-section for the 550-nm transition was not known. Expected characteristics of the transition included

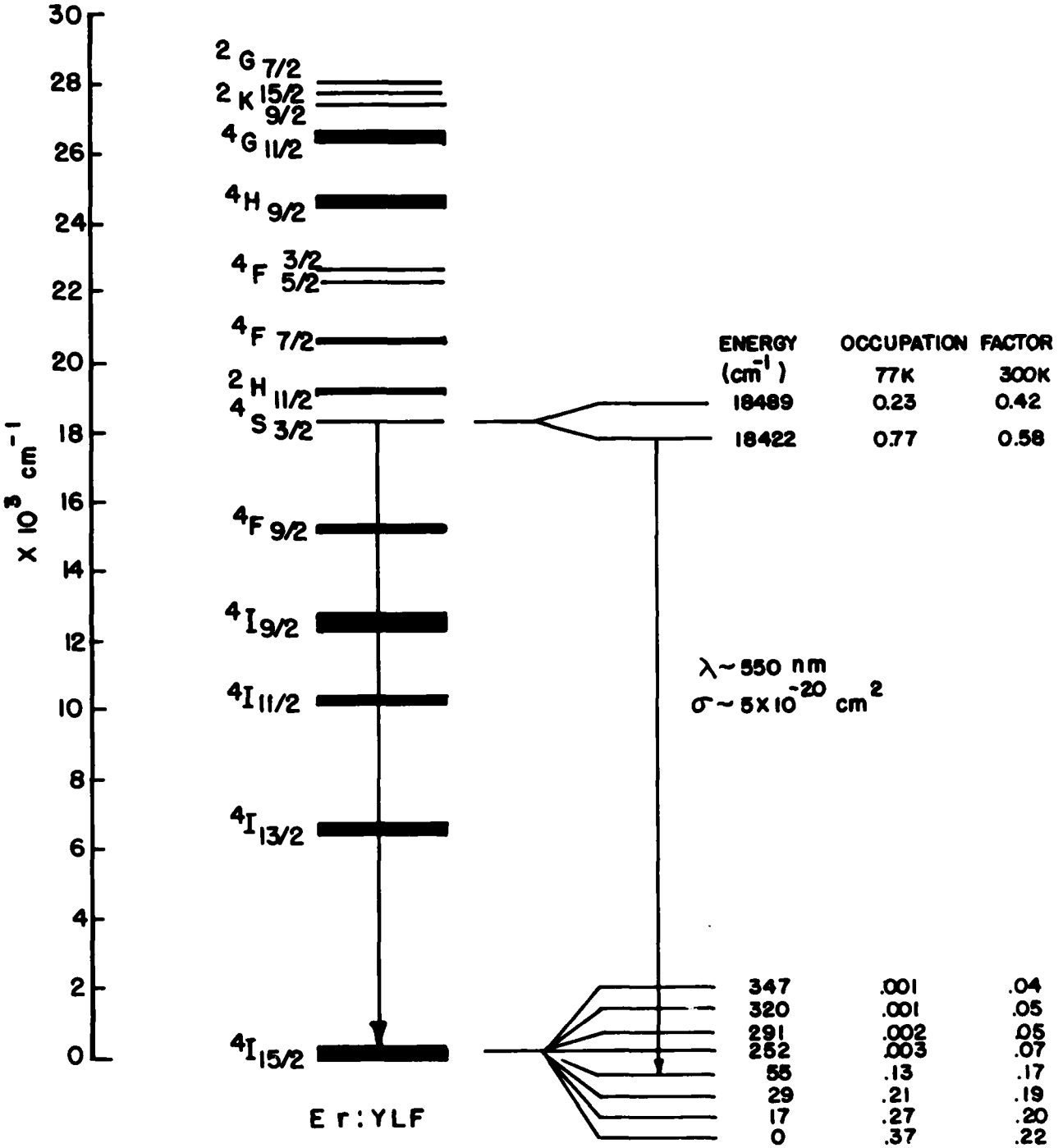

Figure 4.2. Er: Li YF_4 Energy Levels

a stimulated emission cross-section of $8x10^{-20}$ cm^2, an upper level lifetime around 600 μs, and a terminal level relative occupation factor of $1.6x10^{-3}$, all estimated at 77 K. The lasing threshold for the 850 nm transition at 77 K was known to be on the order of 3 J for flashlamp pumping.[14] Room-temperature lasing performance of the 850-nm transition was known to produce typically 100 mJ of output energy with 30 J input to the flashlamp, with threshold energies on the order of 7 J. Slope efficiencies of up to 0.6% had been observed in efforts to optimize the erbium concentration for 850-nm lasing.[14] The fact that the lower laser level for the 550-nm transition was in the ground state manifold was a cause for concern.

Experimental efforts at MIT included the growth of a high-quality boule of $Er:LiYF_4$ with 2% erbium density, the spectroscopic characterization of samples from this boule, particularly the measurement of the 55-nm cross-section at 77 K, and lasing experiments at 77 K using a xenon flashlamp as a pump source.

The growth of $Er:LiYF_4$ proved much more tractable than that of $LiTbF_4$, and the MIT group succeeded in producing a high-quality boule which yielded a 5-mm diameter by 75-mm long laser rod, along with other smaller samples. Cross-section measurements on this material yielded a stimulated emission coefficient of $5x10^{-20}$ cm^2 at 77 K, slightly smaller than the anticipated $8x10^{-20}$ cm^2. Lasing experiments at 77 K produced lasing of the 850 nm transition, $^4S_{3/2} \rightarrow {}^4I_{13/2}$. All efforts to lase the 550-nm transition failed. Although the efficiency of the pump cavity was low, the 550-nm transition was expected to lase, since the 850-nm transition did. Excited state absorption is suspected as an inhibitor of 550-nm lasing.

Efficiency of Low-Temperature Lasers - The operation of solid-state materials at temperatures well below ambient affects the efficiency of the laser in at least three ways. The first effect is the reason for reducing temperature: increased cross-section, reduced threshold, or some similar effect which improves the lasing operation of the material. The second and third effects are the costs. Low-temperature pump cavities are necessarily more complex than room temperature cavities, and often less efficient as a result. Also, the power required to operate the refrigeration system required

for low-temperature operation can become appreciable for situations in which a large amount of heat must be extracted from a laser crystal held at low temperatures. One attempts, by careful pump cavity design, to minimize the first cost. The cooling penalty cannot always be entirely avoided, however. This section will discuss some implications of low temperature operation on the Tb and Er-doped rare-earth materials studied.

One way to evaluate the refrigeration problem is to scale all energy transfers to the power supplied to the lamp pumping the solid-state material. If:

P_{in} = power input to lamp [watts]

P_R = power supplied to the refrigeration system to hold the laser crystal at operating temperature [watts]

P_o = power output of the laser [watts]

P_H = power evolved as heat in the laser rod [watts]

ε_L = efficiency of the laser based on lamp input alone [0-1]

ε_R = energy efficiency of the refrigeration system [0-∞]

ε_H = efficiency of heat generation in the laser due to optical pumping by the lamp [0-1]

ε = overall laser efficiency including refrigeration [0-1]

then the heat evolved in the laser rod is :

$$P_H = \varepsilon_H P_{in} \tag{4.1}$$

and the refrigeration power required to extract this heat is:

$$P_R = \frac{P_H}{\varepsilon_R} = \frac{\varepsilon_H P_{in}}{\varepsilon_R} \tag{4.2}$$

and the overall efficiency is:

$$\varepsilon = \frac{P_o}{P_{in} + P_R} = \frac{\varepsilon_L P_{in}}{P_{in} + \frac{\varepsilon_H P_{in}}{\varepsilon_R}} = \frac{\varepsilon_L}{1 + \frac{\varepsilon_H}{\varepsilon_R}} \tag{4.3}$$

Thus, the quantity $\frac{\varepsilon_H}{\varepsilon_R}$ describes the efficiency penalty of refrigeration. In general, all of ε_L, ε_H, ε_R are functions of temperature and of laser material. We will make simple estimates of these quantities for the materials and conditions of this investigation.

a. Refrigeration Efficiency ε_R: An upper limit to this quantity is set by the thermodynamic efficiency [15]

$$\varepsilon_R = \frac{T_c}{T_h - T_c} \tag{4.4}$$

in which: ε_R = refrigeration efficiency, numerically equal to the heat power extracted from load at temperature T_c by 1 watt of supplied power

T_c = temperature of refrigerated crystal [K]

T_h = temperature at which heat extracted from crystal is "dumped" [K]

Table 4.2 lists thermodynamic ε_R as a function of T_c, with T_h = 300°K.

TABLE 4.2

THERMODYNAMIC REFRIGERATION EFFICIENCY FOR T_h = 300 K

T_C[°K]	ε_R (0-∞)
250	5
200	2
150	1
100	0.5
50	0.2

For comparison, table 4.3 lists the performance of two different refrigeration systems and compares their efficiencies with thermodynamic values.

TABLE 4.3

COMMERCIAL REFRIGERATION UNITS

Unit	T_C [°K]	Heat Extracted [Watts]	Power Required [Watts]	ε_R	Percent of Thermodynamic ε_R
Neslab	250	500	3960	0.12	2.4
ULT-80 [16]	230	300	3960	0.075	2.3
Air Products	150	175	5000	0.035	3.5
CS-180 [17]	77	100	5000	0.02	5.8

The efficiencies of these units are much smaller than thermodynamic limits.

b. Heat Generation Efficiency ε_H - Heat is generated in the refigerated region of the pump cavity due to absorption of flashlamp light and by conduction from warmer neighboring assemblies which are imperfectly insulated from the refrigerated section. Heat evolution in the laser rod itself arises from the fraction of absorbed flashlamp energy which does not produce population inversion. Absorption in the coolant liquid and in flow tubes also produces heat which must be removed by the refrigeration system to maintain the temperature of the laser rod. Koechner[18] measured these absorption efficiencies for a high power, CW-pumped Nd:YAG laser cooled by distilled water. He found that 5% of the pump lamp power was dissipated as heat by the laser rod, and that an additional 7% was dissipated as heat in the coolant and flow tubes. The lasing efficiency was 2%, a high efficiency for Nd:YAG. These fractions can be expected to vary for different coolants, lasing materials, and pump cavity designs, but they given an indication of the range of values to expect. For this example, 12% of the lamp energy is dissipated by the rod, coolant, and flow tubes, giving $\varepsilon_H = 0.12$.

The ratio $\varepsilon/\varepsilon_L$ (equation 4.3) measures the effect of refrigeration power requirements on the efficiency of a refrigerated laser device. This ratio is plotted in figure 4.3 for temperatures from 70 K to 250 K and four values of heat evolution efficiency ε_H. Refrigeration efficiency was 5% of the thermodynamic value for each temperature. For the most favorable combination of conditions, 250°K and $\varepsilon_H = 0.05$, $\varepsilon/\varepsilon_L = 0.833$. If ε_L increases by more than 20% at 250°C (relative to room temperature), a net gain in efficiency is obtained by reducing the temperature. For the least favorable case $\varepsilon/\varepsilon_L = 0.071$ at 70 K, and a more than 14-fold increase in ε_L compared to room temperature is necessary to justify cooling.

In evaluating cryogenic laser materials which emit directly in the green, the ratio $\varepsilon/\varepsilon_L$ can be compared to the conversion efficiency of nonlinear crystals which convert 1.06 μm radiation to 532 nm radiation in frequency-doubled Nd:YAG lasers. Typically, this conversion efficiency ranges from 10% to 25% for reliable, long-term operation of the doubling crystal. The refrigeration requirement in the first case and the frequency doubling requirement in the second case both reduce the total efficiency of the laser system below that of the laser itself. In figure 4.3, the ratio $\varepsilon/\varepsilon_L$ exceeds 0.25 for a significant range of temperature and ε_H, and in this range cooling could be a viable alternative to frequency doubling. However, the lasing efficiency (ε_L) of the cooled material must still be taken into account.

Consider, for example, the use of three solid state materials, $LiTbF_4$ at 77 K, Er:$LiYF_4$ at 77 K, and frequency-doubled Nd:YAG at room temperature in a bathymetry laser. This hypothetical bathymetry laser generates 2 mJ pulses in the 510-550 nm wavelength range at a PRF of 2000 Hz, developing 4 W of average power in the green. Pulse width is assumed to be suitably short in all cases.

$LiTbF_4$ - The largest estimate of slope efficiency for $LiTbF_4$ was 3%, requiring 133 W above threshold to generate 4 W of output at 545 nm. The lowest threshold estimate was 1.52 kW in CW pumping (table 4.1). Assuming that CW-pumped, repetitively Q-switched operation is possible, an input power of 1653 W would generate the 4 W output required. At 77 K with $\varepsilon_H = 0.05$, the total power required would be 5785 W including refrigeration.

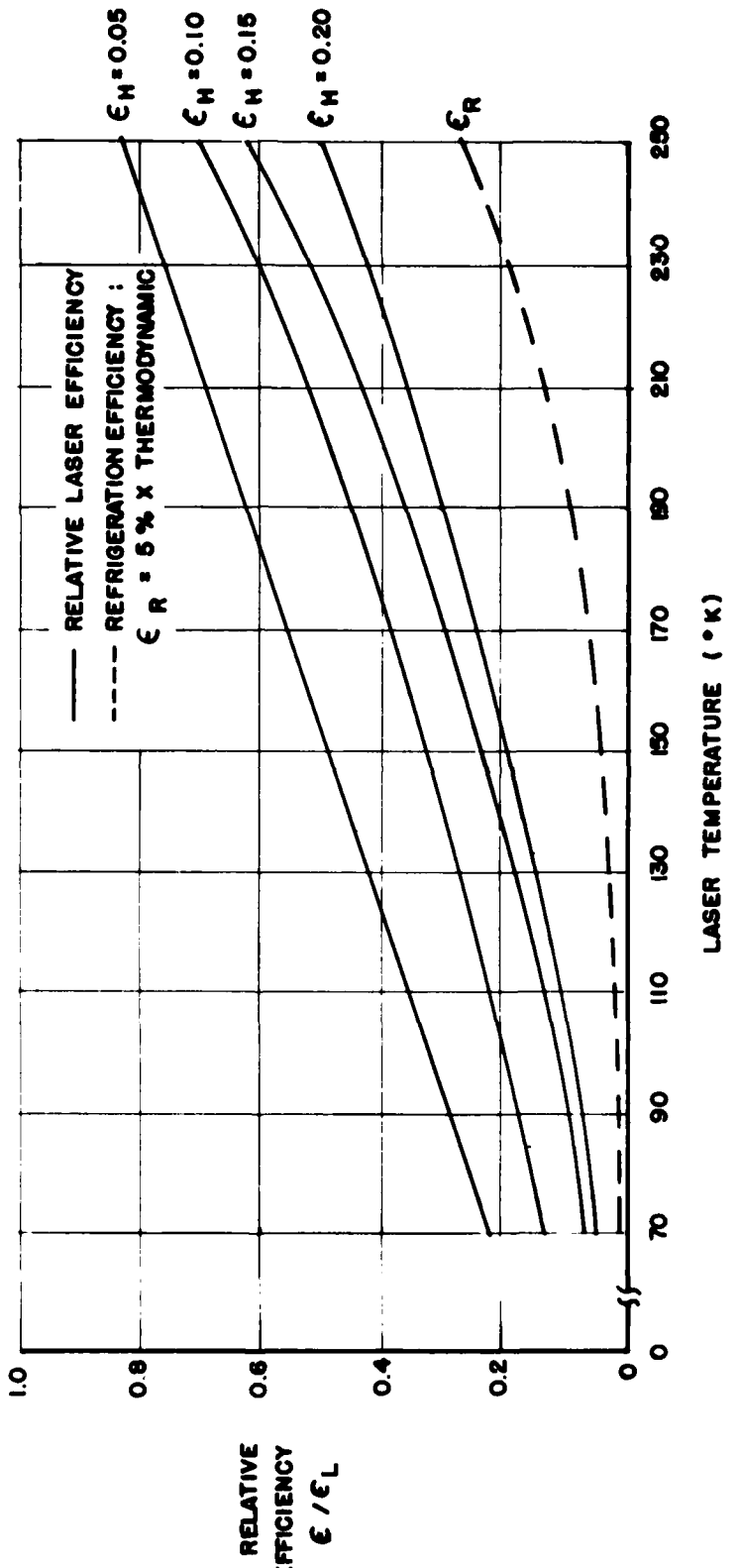

Figure 4.3. Relative Efficiency ϵ/ϵ_L Versus Temperature For Selected Values Of ϵ_H

Er:$LiYF_4$ - Pulsed thresholds for this material's 850-nm transition were estimated at approximately 3 J. Assume that a 1 J threshold for the 550-nm transition is possible at 77 K, and that 3% slope efficiency is possible. Then at 2000 Hz, 2133 W of pumping power would produce 4 W of output power. Including refrigeration power brings the total up to 8332 watts, for operation at 77 K, refrigeration at 5% of thermodynamic efficiency, and $\varepsilon_H = 0.05$.

c. Frequency-Doubled ND:YAG - 1.06 μm ND:YAG lasers operate with maximum efficiencies of about 2% in both Q-switched and CW operation. A conservatively operated doubling crystal would convert 10% of the laser output to 532 nm, for an overall efficiency of 0.2%. Such a laser would generate 40 W at 1.06 μm, convert 4 W to 532 nm, and consume 2000 W of prime power. It should be emphasized that a 40 W, 2-KHz Q-switched Nd:YAG laser represents a significant technical challenge itself. In this sense, the 0.2% efficiency must be considered an upper bound.

Table 4.4 summarizes the estimates just discussed.

TABLE 4.4

COMPARISON OF $LiTbF_4$, Er:$LiYF_4$, AND FD Nd:YAG AS 4-WATT, 2000 Hz BATHYMETRY LASERS

Material	λ[nm]	Pump Power Input [W]	Total Power Input [W]
$LiTbF_4$	545	1653	5785
ER:$LiYF_4$	550	2133	8332
FD ND:YAG	532	2000	3000*

*Estimate for cooling and auxiliary electronics

The estimates for the Tb and Er materials used "best-case" estimates of slope efficiency, lasing threshold, and heat evolution efficiency. Even under these conditions, over 90% of the required pumping power serves to bring the laser to threshold, and less than 10% of the pump power keeps the laser far enough above threshold to generate 4 W of output power. This division of power makes a low lasing threshold a primary criterion for a practical cryogenic laser. In the estimates on Tb and Er, a threshold power on the order of hundreds of watts instead of thousands of watts would have drastically decreased the total power required.

The MIT studies of growth and spectroscopy in $LiTbF_4$ and $Er:LiYF_4$ provided concrete information needed to evaluate the materials as cryogenically operated green lasers. $LiTbF_4$ proved extremely difficult to grow, and it was not possible to produce a 10 cm long laser rod. In addition, its stimulated cross-section at 77 K was $1.1x10^{-21}$ cm^2, less than a tenth the expected value. This small cross-section would produce prohibitively high lasing thresholds. Growth problems were not encountered with $Er:LiYF_4$, and its cross-section at 550 nm was $5x10^{-20}$ cm^2, close to the expected value. The material lased at 850 nm at 77 K, but not at 550 nm. This result indicates some obstacle in the material to 550 nm lasing, possibly excited state absorption. The analysis of refrigerated lasing efficiency indicated that even with optimistic assumptions about performance, both materials would be less efficient at 77 K than frequency-doubled Nd:YAG at room temperature.

The analysis of refrigerated operation showed that the power consumed by the refrigeration system can exceed the power required to pump the laser, particularly at temperature approaching 77 K. In general, refrigerated operation makes the most sense in situations where the heat power extracted at low temperatures is small. In many solid-state lasers including the ones discussed here, most of the pumping power supplied to the laser serves to bring the laser to threshold, and only a small amount of additional power is necessary to maintain above-threshold operation. In such situations, a low lasing threshold at the cryogenic operating temperature is essential for efficient operation.

The data presented in figure 4.3 give an indication of the efficiency required of a cryogenic lasing material. For example, at 70 K and with $\varepsilon_H = 0.05$, a lasing efficiency (ε_L) of 4.29% is required to produce an overall efficiency of 1%. Under the same conditions, an ε_L of 0.85% would produce an overall efficiency of 0.2%, the efficiency assigned to the frequency-doubled Nd:YAG laser. Thus, at 77 K, a green-emitting solid-state material with an efficiency in the 1%-4% range would represent an overall improvement in efficiency over frequency-doubled Nd:YAG. For airborne systems applications, other factors such as the size and weight of the cryogenic apparatus, and its reliability and maintainability in field conditions must be considered along with efficiency.

SECTION 5

CONCLUSIONS

This report has described the basic characteristics of four low-temperature lasing transitions, and considered their utility for naval optical communications and hydrography systems. Lasing results were obtained for the 946-nm transition in Nd:YAG, and serious obstacles to efficient operation were identified for $LiHoF_4$, $LiTbF_4$, and Er:$LiYF_4$. An elliptical pump cavity capable of maintaining a 5-mm x 75-mm laser rod at temperatures of 210 K was developed, and valuable experience with low-temperature lasing was acquired. A basic analysis of the power consumption of refrigerated solid-state lasers showed that a green-emitting solid-state material lasing at a temperature of 77 K could be more efficient than frequency-doubled Nd:YAG if its lasing efficiency exceeded 1%, and if its heat evolution efficiency was 5% or less.

None of the transitions studied showed a clear improvement over 532 nm Nd:YAG for either system application. The limitations of the rare-earth fluoride materials appear difficult to alleviate. $LiHoF_4$ suffers from resonant pumping of its lower laser level, which obviates much of the advantage of its 4-level structure. The lifetime of the upper level is 33 μs at 77 K, which limits the energy storage for Q-switching and requires pumping pulses which are short for flashlamps, and not conducive to long lamp life. $LiTbF_4$ appears to be difficult to grow in the size and optical quality required for laser rods. Both $LiTbF_4$ and Er:$LiYF_4$ appear to have thresholds too high for efficient operation at 77 K.

The 946-nm transition in Nd:YAG produced a significant amount of energy, 42 mJ, at a temperature of 210 K. The temperature dependence of threshold agreed fairly well with a simple rate-equation model. The major question for this transition is whether the inversion energy can be extracted at 946 nm. Extraction at 1.06 μm clearly occurs: the laser rod generated 270 mJ at 1.06 μm when pumped at the energy level (34.2 J) which produced 42 mJ at 946 nm.

The reasons for the lower extraction efficiency at 946 nm are not entirely clear. The smaller stimulated emission cross-section at 946 nm reduces the extraction rate compared to all competing processes. Amplified spontaneous emission at 1.06 μm occurs to some extent according to the fluorescence data. The intensity of ASE may or may not account for all the missing energy. Excited state absorption presents another explanation, but is not consistent with the energy level structure of the Nd^{+3} ion. If the explanation for the low oscillator efficiency lies in slow extraction of energy at 946 nm compared to competing loss processes, an oscillator-amplifier configuration may be capable of significantly higher efficiency.

Further fluorescence measurements at low temperatures would clarify some questions about the results reported here. It is not at all clear why the 1.06 μm and 946 nm spontaneous emission intensities decay with different time constants, or why the time constants have different dependencies on pump energy.

Determination of the ultimate efficiency of the 946-nm transition would permit a straightforward comparison with the 1.06-μm Nd:YAG transition. If, for a prescribed amount of input power, the 946-nm laser could produce enough energy at 473 nm (after frequency doubling) to provide extended range compared to that available at 532 nm from the same power input, then it is advantageous to use the 946-nm transition.

The basic analysis of cooling shows that the power consumed by the refrigeration system can exceed the power required to pump optically a low-temperature material. Lasing efficiency becomes especially crucial in this type of operation. Minimizing the heat evolved at the low temperature and maximizing the efficiency of the refrigeration system can strongly affect the overall efficiency of a low-temperature laser. Spectrally selective pumping techniques with efficient pump sources can reduce the heat evolution in the laser material. One example of this technique is the use of GaAlAs injection laser diodes to pump the near-IR excitation band of Nd:YAG.

In the course of developing low-temperature laser devices for field application, many scientific and engineering issues must be addressed. This report has explored some of these issues in the context of evaluating Nd:YAG, $LiHoF_4$, $LiTbF_4$, and $Er:LiYF_4$ for possible use in naval communications and bathymetry systems. While none of the materials show a clear advantage over 532-nm frequency-doubled Nd:YAG, the 946-nm Nd:YAG transition may prove efficient enough to merit development for applications in which its shorter wavelength becomes important.

SECTION 6

REFERENCES

1. "Naval Air Development Center Independent Research and Independent Exploratory Development Annual Report FY-81," Report symbol NAVMAT 3920-1, 15 Jan 1982, p 14
2. Singh, S., Smith, R. G., and Van Uitert, "Stimulated-Emission Cross-section and Fluorescent Quantum Efficiency of Nd^{3+} in Yttrium Aluminum Garnet at Room Temperature," Phys Rev B, Vol 10, No. 6, p 2566ff, 15 Sep 1974
3. Marling, Jack, "1.05-1.44 μm Tunability and Performance of the CW Nd^{+3}:YAG Laser," IEEE Journal of Quantum Electronics, Vol QE-14, No. 1, p 56, 1 Jan 1978
4. Wallace, R. W. and Harris, S. E., "Oscillation and Doubling of the 0.946 μm Line in Nd^{3+}YAG," Applied Physics Letters, Vol 15, No. 4, p 111, 15 Aug 1969
5. Vuylsteke, A. A., J. Appl Phys, Vol 34, 1615 (1963)
6. Yariv, A., Introduction to Optical Electronics, Holt, Rinehart and Winston, New York, p 100 (1971)
7. Suggested to us by Dr. H. P. Jenssen of MIT
8. Morozov, A. M., Podkolzina I. G., Tkachuk, A. M, Fedorov, V. A., and Feofilov, P. P., "Luminescence and Induced Emission in Lithium-Erbium and Lithium-Holmium Binary Fluorides," Optics and Spectroscopy, Vol 39, No. 3, (p 338) Sep 1975
9. Podkolzina, I. G., Tkachuk, A. M., Fedorov, V. A., and Feofilov, P. P., "Miltifrequency Generation of Stimulated Emission of Ho^{3+} Ion in $LiYF_4$ Crystals," Optics and Spectroscopy, Vol 40, No. 1, (p 112) Jan 1976
10. Jenssen, H. P., "Preliminary report on $LiHoF_4$ - A 980-nm Laser Candidate," Unpublished draft dtd Sep 1979
11. Linz, A., Jenssen, H. P, Gabbe, D. R., Castleberry, D., and Douma, M. H., "Blue-Green Laser Material," MIT Crystal Physics Laboratory Tech Report No. 17, ONR Contract No. N00014-67-A-0204-0044 (30 May 1974)
12. Goncz, John H. and Newell, P. Bruce, "Spectra of Pulsed and Continuous Xenon Discharges," J Opt Soc Am, Vol 56, No. 1, 87-92, Jan 1966
13. Fan, Tso Yee, "Spectroscopy of $LiTbF_4$," Bachelor of Science thesis prepared in the MIT department of Electrical Engineering, May 1981

14. Chicklis, E. P., Folweiler, R. C., and Naiman, C. S., "High Radiance Er:YLF Illuminator," Sanders Associates Memo No. 1-1412-L-75-429, p 4, Apr 1975

15. Callen, H. B, Thermodynamics, John Wiley and Sons, New York (1960), p 75

16. Neslab Instruments, Inc., 871 Islington St, Portsmouth NH 03801

17. Air Products and Chemicals, Inc., APD-Cryogenics, P.O. Box 2802, Allentown, PA 18105

18. Koechner, Walter, Solid-State Laser Engineering, Springer-Verlag, New York, (1976) p 324

SECTION 7

ACKNOWLEDGEMENTS

The authors thank Mr. Paul Bailey for the design of the low-temperature pump cavity used in this work. The contributions of Mr. Eric Hellmann and Mr. Daniel Lorenzetti in the experiments are appreciated. Mr Francis McMahon contributed ably to the analysis of the Nd^{+3} spontaneous emission data.

The authors gratefully acknowledge the contributions of Dr. Hans P. Jenssen and his colleagues in the Crystal Physics and Optical Electronics Laboratory of the Massachusetts Institute of Technology (MIT) in the area of rare-earth fluorides. Unpublished results of their researches on several materials are discussed in this report. The efforts at MIT were primarily funded by the office of Naval Research-Boston Branch Office. It is a pleasure to acknowledge the contributions of Dr. Matthew B. White of that office to the work reported in these pages.

One of the authors (MBR) wishes to acknowledge the influence on this report of a stimulating sabbatical at Drexel University. The hospitality of the Drexel Department of Physics and Atmospheric Science and the financial support of the NAVAIRDEVCEN Advanced Graduate Study Program are gratefully appreciated.

The authors thank Mr. Paul Moser for his careful reading of the manuscript, and Ms. Janice Strozier and Ms. Jean Eichert for their care and patience in typing it.

APPENDIX A

1. Calculation of Pumping Rates for the $^4F_{3/2}$ Manifold of Nd:YAG

K was estimated from measurement of the threshold energy of the 1.06 μm transition in the pumping apparatus used for the 946 nm lasing tests. Threshold was measured for a simple resonator configuration in which the transmission of the output mirror (near 50%) was the dominant loss factor. This factor was used in equation (2.3) to compute N_u for the strongest 1.06-μm transition, $R_2 \rightarrow Y_3$, which was assumed to be the only transition active at threshold. This value of N_u and the measured threshold energy determine the value of K in equation (2.1).

This determination of K actually applies to the density N_{R2} of the R_2 component of the $^4F_{3/2}$ manifold. To compute a value for the density N_{R1} of the R_1 component, we assumed that the two components were in thermal equilibrium, so that

$$\frac{N_{R2}}{N_{R1}} = e^{-\frac{83\ cm^{-1}}{k\ T}} \qquad (A.1)$$

Then

$$K_{R1} = K_{R2}\ e^{\frac{83\ cm^{-1}}{kT}} \qquad (A.2)$$

is the pumping rate (called K in the main text) for the upper level of the 946 nm transition.

As an example, a 1.06-μm threshold energy of 2.75 J was measured in a 1.06 μm resonator with an output reflectance of 45%. Other values for equation (2.3) were:

$$\sigma = 4.6\text{x}10^{-19}\ \text{cm}^2$$

$$\ell = 6.35\ \text{cm}$$

$$R = 0.45$$

$$T_E = 1.0$$

$$\alpha = 2\text{x}10^{-3}\ \text{cm}^{-1}$$

Then, from equation (2.3), $N_u = N_{R2} = 1.41\text{x}10^{17}$ ions/cm^3 at threshold, and from equation (2.1), $K_{R2} = 5.12\text{x}10^{16}$ ions/cm^3-joule, and from equation (I.2), $K_{R1} = 9.07\text{x}10^{16}$ ions/cm^3-joule at 210 C.

2. Partition Function for the $^4I_{9/2}$ Manifold

In calculating the Z(T) used in equation (2.3), only the five components of the $^4I_{9/2}$ manifold were used, since thermal population of higher levels is negligible. The form used was

$$Z(T) = \sum_{i=1}^{5} \exp[-\varepsilon_i/kT] \qquad (I.3)$$

in which ε_i is the energy of the ith component of $^4I_{9/2}$, k is Boltzmann's constant and T is absolute temperature. Representative values are:

Table A.1. Partition Function for Nd $^4I_{9/2}$ Manifold

T[K]	Z(T)
200	1.73
210	1.78
220	1.82
230	1.87
240	1.91
250	1.96
260	2.00
270	2.04

This Page Intentionally Left Blank


4-
DT